THESIS FOR THE DEGREE OF DOCTOR OF PHILOSOPHY

Communication and Positioning Uncertainties in Cooperative Intelligent Transportation Systems

Erik Steinmetz

CHALMERS
UNIVERSITY OF TECHNOLOGY

Communication Systems Group
Department of Electrical Engineering
Chalmers University of Technology
Gothenburg, Sweden, 2019

Communication and Positioning Uncertainties in Cooperative Intelligent Transportation Systems

Erik Steinmetz
ISBN 978-91-7905-111-2

Doktorsavhandlingar vid Chalmers tekniska högskola
Ny serie Nr 4578
ISSN 0346-718X

Communication Systems Group
Department of Electrical Engineering
Chalmers University of Technology
SE-412 96 Gothenburg, Sweden
Phone: +46 (0)31 772 1000
Email: estein@chalmers.se

Division of Safety and Transport
RISE Research Institutes of Sweden
Box 857, Borås, Sweden
Phone: +46 (0)10 516 5000
Email: erik.steinmetz@ri.se

Front cover:
Illustration of the importance of reliable communication and positioning in cooperative intelligent transportation systems.

Typeset by the author using LaTeX

Printed by Chalmers Digital Print
Gothenburg, Sweden, May 2019

Abstract

The current road transport system has problems with both safety and efficiency. Future intelligent transportation systems (ITS) are envisioned to alleviate these problems. In particular, cooperative ITS, where vehicles are connected to each other and the cloud, will allow vehicles to collaborate and share both sensor and control information. This will significantly expand the possibilities of optimizing traffic flow and increasing safety. However, as both communication and sensing are unreliable, a key challenge in cooperative ITS is how to accommodate for communication and sensing impairments. This requires an understanding of what the limitations of communication and sensing systems are, and how their uncertainties affect the control and coordination task. The contribution of this thesis lies on the intersection of the fields of communication, sensing, and control, and can be summarized as follows.

First of all, through the use of stochastic geometry, we analyze the impact of interference in vehicular networks, and propose a general procedure to analytically determine key performance metrics such as packet reception probabilities and throughput. Along with this procedure, we provide a model repository that can be used to adapt to both rural and urban propagation characteristics, and different medium access control protocols. The procedure can be used to gain fundamental insights about the performance of vehicular communication systems in a variety of scenarios of practical relevance.

Secondly, when it comes to sensing uncertainties, we use Fisher information theory to provide bounds on the achievable performance of cooperative positioning solutions. We thereby characterize how the composition of the vehicle fleet, and the penetration rate of vehicles with extensive sensing capabilities affects positioning and mapping performance. While the analysis is generally applicable, we present simulation results from a multi-lane freeway scenario, which indicate that introducing a small fraction of cooperating vehicles with high-end sensors significantly improves the positioning quality of the entire fleet, but may not be enough to meet the stringent demands posed by safety-critical applications.

Finally, we study how communication and sensing uncertainties impact cooperative intersection coordination. We show that the requirements on control, communication and sensing are stringent if they are treated separately and that they could be relaxed if the individual systems are made aware of each other. This awareness is explored in two ways: we provide a communication system analysis for a centralized intersection coordination scheme using stochastic geometry, which can be used to provide guidelines on how to design the communication system to guarantee a control-dependent communication quality. We also propose a collision aware resource allocation strategy, which proactively reduces channel congestion by only assigning communication resources to vehicles that are in critical configurations, i.e., when there is a risk for future collisions.

This thesis, through the use of several mathematical tools, thus sheds new insights into the communication, sensing and control performance of cooperative ITS.

Keywords: cooperative intelligent transportation systems, vehicular communication, packet reliability, resource allocation, cooperative positioning.

List of Publications

This thesis is based on the following publications:

(A) E. Steinmetz, M. Wildemeersch, and H. Wymeersch, "WiP Abstract: Reception Probability Model for Vehicular Ad-Hoc Networks in the Vicinity of Intersections," in *Proceedings of the ACM/IEEE 5th International Conference on Cyber-Physical Systems (ICCPS)*, Berlin, Germany, Apr. 2014, pp. 223.

(B) E. Steinmetz, R. Hult, G. Rodrigues de Campos, M. Wildemeersch, P. Falcone, and H. Wymeersch, "Communication Analysis for Centralized Intersection Crossing Coordination," in *Proceedings of 11th International Symposium on Wireless Communications Systems (ISWCS)*, Barcelona, Spain, Aug. 2014, pp. 813–818.

(C) E. Steinmetz, M. Wildemeersch, T. Q. S. Quek, and H. Wymeersch, "A Stochastic Geometry Model for Vehicular Communication near Intersections," in *Proceedings of IEEE Globecom Workshops (GC Wkshps)*, San Diego, USA, Dec. 2015.

(D) E. Steinmetz, M. Wildemeersch, T. Q. S. Quek, and H. Wymeersch, "Packet Reception Probabilities in Vehicular Communications Close to Intersections," submitted to *IEEE Transactions on Intelligent Transportation Systems*, 2018.

(E) R. Hult, G. Rodrigues de Campos, E. Steinmetz, L. Hammarstrand, P. Falcone, and H.Wymeersch, "Coordination of Cooperative Autonomous Vehicles: Toward safer and more efficient road transportation," in *IEEE Signal Processing Magazine*, vol. 33, no. 6, pp. 74–84, Nov. 2016.

(F) E. Steinmetz, R. Hult, Z. Zou, R. Emardson, F. Brännström, P. Falcone, and H. Wymeersch, "Collision-Aware Communication for Intersection Management of Automated Vehicles," in *IEEE Access*, vol. 6, pp. 77359–77371, 2018.

(G) E. Steinmetz, R. Emardson, F. Brännström, and H. Wymeersch, "Theoretical Limits on Cooperative Positioning in Mixed Traffic," in *IEEE Access*, vol. 7, pp. 49712–49725, 2019.

Publications by the author not included in the thesis:

(a) E. Steinmetz, R. Emardson, and P. Jarlemark, "Improved Vehicle Parameter Estimation Using Sensor Fusion by Kalman Filtering" in *Proceedings of the XIX IMEKO World Congress on Fundamental and Applied Metrology*, Lisabon, Portugal, Sep. 2009.

(b) J. Bärgman, H. Gellerman, J. Kovaceva, and R. Nisslert, . Selpi, E. Steinmetz, and M. Dozza, "On data security and analysis platforms for analysis of naturalistic driving data" in *Proceedings of the 8th European Congress and Exhibition on Intelligent Transportation Systems and Services*, Lyon, France, Jun. 2011.

(c) C. Ahlstrom, T. Victor, C. Wege, and E. Steinmetz, "Processing of Eye/Head-Tracking Data in Large-Scale Naturalistic Driving Data Sets," *IEEE Transactions on Intelligent Transportation Systems*, vol. 13, no. 2, pp. 553–564, 2012.

(d) K. Westlund, P. Jönsson, S. Bergstrand, and E. Steinmetz, "Evaluation of Navigation Satellite Systems for Forestry and its Precision in a Forest Environment," in *Proceedings of the 45th International Symposium on Forestry Mechanisation*, Dubrovnik,Croatia, Oct. 2012.

(e) E. Steinmetz, P. Jarlemark, R. Emardson, H. Skoogh, and M. Herbertsson, "Assessment of GPS derived speed for verification of speed measuring devices," *International Journal of Instrumentation Technology (IJIT)*, vol. 1, no. 3, pp. 212–227, 2014.

(f) M. Abdulla, E. Steinmetz, and H. Wymeersch, "Vehicle-to-Vehicle Communications with Urban Intersection Path Loss Models," in *Proceedings of IEEE Globecom Workshops (GC Wkshps)*, Washington, DC, USA, Dec. 2016.

(g) B. Peng, G. Seco-Granados, E. Steinmetz, M. Fröhle, and H. Wymeersch, "Decentralized Scheduling for Cooperative Localization with Deep Reinforcement Learning," to appear in *IEEE Transactions on Vehicular Technology*, vol. 68, no. 5, 2019.

Acknowledgments

The path might not have been straight, but now I finally stand on the top of Mount Research. This is to all of you that have made this expedition possible, enjoyable, and believed in me during difficult times.

First of all, I would like to express my deepest gratitude to my main supervisor Prof. Henk Wymeersch. I really appreciate your enthusiastic and supportive approach to supervision, and for how you patiently have thought me what it means to be a researcher.

A big thanks also goes to my co-supervisors Prof. Fredrik Brännström and Dr. Ragne Emardson for fruitful discussions and valuable feedback.

I would also like to thank my colleagues at RISE Research Institute of Sweden. In particular, Jan Johansson and Sven-Christan Ebenhag for making this possible and believing in me!

Also thanks to both former and present colleagues at the Department of Electrical Engineering for the fantastic and stimulating work environment, and all the fun we have had over the years. It has been a pleasure to get to know you all!

Furthermore, I would like to thank all the people that I had the opportunity to work with. A special thanks goes to Matthias Wildemeersch for always being positive and helping me to understand the intricacies of stochastic geometry.

I'm also grateful for all the support and love that I have received from family and friends during these years. Especially you Johanna, and William. Thanks for always being there, making me smile, and giving me the energy to complete this project.

Erik Steinmetz
Göteborg, May 2019

Financial support

This work is supported, in part, by the National Metrology Institute hosted at RISE Research Institutes of Sweden, which in turn is partly funded by VINNOVA under the program for national metrology (grant no. 2015-06478); the PRoPART (Precise and Robust Positioning for Automated Road Transport) project, funded by the European GNSS Agency under the EU H2020 program (grant no. 776307).

Contents

Part I

Overview

CHAPTER 1

Introduction

1.1 Background and Challenges

The road transport system as we know it today has large problems with both safety and efficiency. For instance, the number of traffic related deaths per year continues to climb, and reached a staggering 1.35 million in 2016 [1]. This makes it the main cause of death among children and young adults aged 5-29 years and the ninth among all age groups. Furthermore, many of the major cities around the world are locked down by traffic congestion during rush hour, and it is reported [2] that the U.S. alone wastes 11.7 billion liters of gas annually due to congestions, which together with productivity losses is estimated to cost the society more than 160 billion dollars per year. Moreover, about 14 % of the global emissions of anthropogenic greenhouse gases (e.g., CO2) comes from the transport sector [3]. This shows that the current road transport system not only has large impact on our health, quality of life and economy, but also on the environment.

To alleviate these problems, one of the main objectives in future intelligent transportation systems (ITS), is essentially, to control or coordinate vehicles in a safe and efficient manner. Thus, we have during the last decades seen how the automotive industry have shifted focus, first from passive to active safety as well as advanced driver assistance systems (ADAS), and then moved aggressively towards autonomous and self-driving vehicle technologies. Along with this, vehicles have also been equipped with more advanced sensors (such as global navigation satellite systems (GNSS) receivers, radars, LIDARs and cameras) for observation both of the own state (e.g., position and velocity) and sensing of other objects in the dynamically changing environment. However, as the situational awareness in an autonomous vehicle is limited to the field of view (FOV) of its on-board

sensors and map-based context information, the possibility to optimize its motion in regards to the surrounding traffic situation is limited. To extend the situational awareness beyond the FOV of traditional on-board sensors, and to harness the full potential of the technological revolution, it is thus natural to move from autonomous to cooperative ITS. A key enabler for cooperative ITS is wireless communication, and by being connected [4]–[7] to both each other and the cloud, vehicles and road side infrastructure are expected to collaborate. In particular, vehicles are foreseen to cooperate when it comes to coordination and control [8], [9] and for sensing and perception [10], [11], where the latter in principle is an enabler of the former, as an accurate representation of the surrounding environment is key when it comes to achieving safe and efficient control. We can thus say that cooperative ITS relies on the three pillars control, sensing and communication, and that there are clear dependencies between these as illustrated in Figure 1.1.

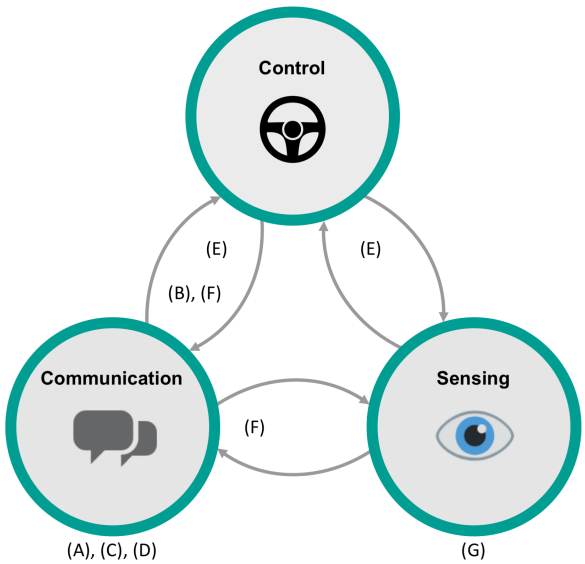

Figure 1.1. Control, sensing and communication, the three pillars that together realizes cooperative ITS. The arrows illustrate that they are coupled and that the performance or awareness of one system can have great impact on another. We also illustrate which topics the appended papers pertain to.

The different pillars, which also can be seen as subsystems, or research fields, have been studied extensively within their respective domains. Also, the connections between the different fields have to some extent been explored. The use of robust control formulations that explicitly account for state uncertainties have been considered, e.g., [12]–[16]. Moreover, e.g., [17], [18] have looked at what can be tolerated in terms of network reliability to sustain stability in the controller. There are also works, such as [19]–[22],

that have studied how to allocate communication resources based on awareness of the control system. Nonetheless, knowledge gaps remain. In particular, one of the main challenges, as pointed out in [23], is how to accommodate for communication and sensing uncertainties in safety critical applications such as cooperative automated driving. This is an intricate problem and before we can even think of how to solve this, it is important to understand what the limitations regarding communication systems, and sensing and perception systems, are in the setting of cooperative ITS.

In terms of vehicular communication a large body of research exists [5]–[7]. When it comes to evaluating the performance it is in most cases necessary to turn to either simulations [24]–[26] or measurements campaigns [27]. As these can be both time consuming and scenario specific, there is a need for analytical models that can be used to gain fundamental insights about the performance in different scenarios. In particular, for high velocity scenarios (e.g., highways), and accident prone scenarios (e.g., intersections).

Similarly, the literature is rich regarding cooperative sensing and perception [28]–[35], and much work have for instance been done to characterize the benefit of cooperation when it comes to positioning. In particular, fundamental performance limits [31]–[33], [35], can be used both for benchmarking and provide key insights about what affects the positioning performance. However, out of the works that focus on performance limits only few, e.g., [32], [33], specifically target the vehicular setting. Thus there is a need to better quantify the fundamental performance of cooperative positioning in vehicular networks, especially under the assumptions of realistic sensors such a GNSS, radars and LIDARs. Also, the communication and sensing technologies required for cooperative positioning will be gradually introduced on the market. As highlighted in [36], it is therefore important to gain an understanding of how the composition of the vehicle fleet and the gradual penetration of vehicles with high-end sensors impacts the positioning quality.

1.2 Objectives

This thesis addresses some of the challenges with cooperative ITS outlined above. In particular, we

- propose analytical models for the reliability of packet transmissions in vehicular networks. Mainly, to gain a better understanding of the performance of vehicular communication systems and what uncertainties we have to be able to cope with in cooperative ITS application;

- provide bounds on the achievable performance of cooperative positioning solutions in future ITS, based on a Fisher information theory approach. Using this, we characterize how the sensing capability in a given vehicle fleet affects positioning and mapping performance, and if the obtained accuracies are sufficient to meet the demands of safety critical ITS applications, such as cooperative automated driving;

- characterize how sensing and communication uncertainties impacts safety critical applications, and provide a method to reduce the channel load, by only assigning communication resources to vehicles that are in critical configurations, i.e., when there are risk for future collisions.

1.3 Outline

The thesis is divided in two parts. Part I provides an introduction to basic concepts and tools used in the appended papers. In particular, Chapter 2 gives an overview of vehicular communication and some of its challenges. Furthermore, we introduce the concept of stochastic geometry, which is the main tool used in Papers A-D, and briefly show how it can be used to analyze the impact of interference in a wireless network. In Chapter 3, we provide an introduction to important concepts within the field of positioning, and discuss positioning requirements and sensor technologies from the perspective of ITS. In addition to this, we introduce the concept of Fisher information and Cramér-Rao bounds, and briefly show how these can be used to obtain fundamental insights about the performance of cooperative positioning solutions, which is the main goal of Paper G. In Chapter 4, we give some intuition on how the control problem can be formalized. Also, we review the concept of model predictive control and discuss how communication and sensing uncertainties impact safety critical applications. Chapter 5, summarizes the author contributions and gives directions for future work. Part II of this thesis consists of the appended Papers A-G.

CHAPTER 2

Communication

In this chapter, we give some background on vehicle-to-vehicle (V2V) and vehicle-to-infrastructure (V2I) communication (together referred to as V2X communication). We discuss current standards and technologies and typical characteristics of the vehicular channel as well as some of the underlying reasons for packet drops and random latencies in vehicular networks. Furthermore, we briefly discuss the main challenges that come with using wireless communication for safety critical applications, such as for example an centralized intersection coordination system. Lastly we also introduce the concept of stochastic geometry, which is the main tool used in Papers A-D, and give an example of how it can be used to characterize the packet reception probability in a wireless network.

2.1 Current Standards and Technologies

To meet the communication demands of future ITS applications, both USA and Europe, as well as many other countries, have allocated spectrum in different frequency bands around 5.9 GHz (see Fig. 2.1), and large efforts are put into research and standardization of V2X communication.

The most notable examples are the North American standard, referred to as IEEE wireless access in vehicular environment (WAVE) (which includes both the IEEE 802.11p standard [39], [40] and the higher level standard IEEE 1609 [41]) and the European standard, referred to as ITS G5 [7], [42] which also builds on the lower level standard IEEE 802.11p. The IEEE 802.11p standard is an amendment of the well-known wireless local are network (WLAN) standard IEEE 802.11 modified to the vehicular environment,

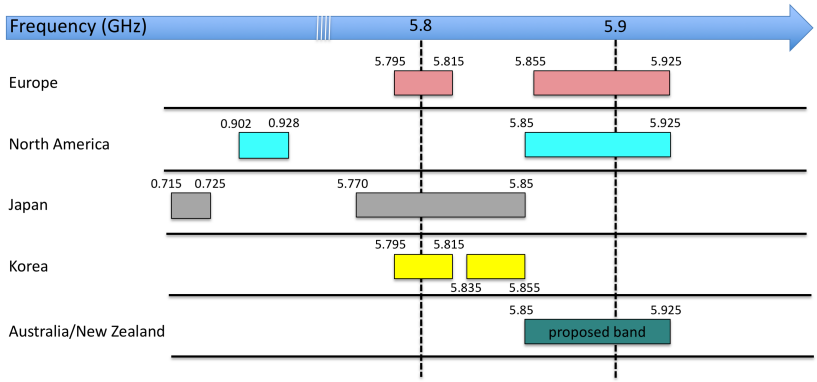

Figure 2.1. Overview of spectrum allocations for ITS applications in different countries (based on information from [37], [38]).

and it specifies the medium access control (MAC) and physical (PHY) sub layers of the protocol stack. The main difference between the amendment and the original standard is that authentication, association and security features are disabled. This allows for ad-hoc communication without overheads associated with setting up the so-called basic service set from traditional WLAN networks, and as can be understood this is a major advantage in vehicular networks as the communication links between rapidly moving vehicles might only exist for a short amount of time. Except for this the PHY and MAC sub-layers are similar to the original 802.11 standard. In particular, the PHY layer relies on orthogonal frequency division multiplexing (OFDM) in 10 MHz channels (i.e., the bandwidth is halved compared to 802.11a) with possible data rates between 3 Mbps and 27 Mbps [43]. The MAC protocol, which governs the channel access is based on a carrier sense multiple access/collision avoidance (CSMA/CA) approach [44], [45]. In simple terms this means that when a node (e.g., vehicle or other road user with communication capability) has a packet to send, it first listens to channel. If the channel is free, the node starts transmitting the packet. If the channel is busy, the node waits a random back-off time before it tries to transmit the packet again.

Using the IEEE 802.11p standard vehicles can broadcast periodic awareness messages, containing core state information such as location, speed and brake status, or event driven hazard messages, over a range of about 300-500 meters [44]. At the moment the message formats have not been harmonized between North America and Europe and a variety of message types exists. The European message standardization is handled by ETSI, and the message set is made up of two types of messages, namely cooperative awareness messages (CAM) and decentralized environmental notification messages (DENM). The CAM are periodic messages (1-10 Hz), while the DENM are event driven hazard warnings. In North America the message are referred to as basic safety messages (BSM), and the

standardization is handled by the Society of Automotive Engineers (SAE). The BSM are periodic (about 10 Hz), but extra information can be included due to event triggers. The size of a CAM/BSM is typically 300-400 bytes [45]. Hence using the default data rate of 6 Mbps it will take around 400-500 μs to transmit a message.

For a more detailed description of the WAVE and ITS G5 standards, the different message types, as well as the history of the standardization process see, e.g., [45], [46].

Worth to mention is also that the fifth generation (5G) cellular systems are being developed to support device-to-device (D2D) communication [47]–[49], and is thus, in combination with traditional cellular services, envisioned to act as an important complement to the above discussed standards. In particular, it has been shown that 5G device-to-device (D2D) is a promising technology capable of boosting the spectrum utilization in ITS applications [50].

2.2 The Vehicular Channel

Vehicular communication systems must be able to function in a multitude of conditions, including both low and high mobility scenarios, as well as rural and urban environments. This means greatly varying channel characteristics, and in order for a receiver (Rx) to correctly decode a message it needs to be able to cope with large/rapid fluctuations in the received signal power, large Doppler shifts, as well as large delay spreads. However, as the work in this thesis focuses on signal-to-interference-plus-noise ratio (SINR) based analysis methods we will mainly discuss channel characteristics from a received signal power point of view.

Variations in received signal power over distance can be categorized into three different groups: 1) *path loss* which mainly is caused by the dissipation of the power radiated by the transmitter (Tx) with distance; 2) *large-scale fading* which is caused by obstacles that shadow, i.e., attenuates the signal power through absorption, scattering and diffraction; 3) *small-scale fading* which is due interference between multipath components from different scatterers in the surroundings as well as Doppler shifts resulting from the mobility of the nodes. Variations in the signal strength due to path loss occur over long distances, while large-scale fading occurs over distances that are proportional to the size of the obstructing object. As a rule of thumb large-scale fading occurs over distances that are large compared to the signal wavelength, while small scale fading variations due to multipath and Doppler occur over very short distances, on the scale of a wavelength. Note that for a stationary Rx the small scale-fading due to a constantly changing environment translates into rapid fluctuations of the received power in time. Most often the observed fluctuations in the received signal strength is a combination of large-scale fading and small-scale fading. Hence, considering a Tx and Rx pair with locations $\mathbf{x}_{\text{tx}}$ and $\mathbf{x}_{\text{rx}}$ the received power can be expressed as

$$P_{\text{r}} = P_{\text{t}} S\, l(\mathbf{x}_{\text{tx}}, \mathbf{x}_{\text{rx}}), \tag{2.1}$$

where P_t is the transmitted power, S is the fading, and $l(\mathbf{x}_\mathrm{tx}, \mathbf{x}_\mathrm{rx})$ is the path loss.

To characterize the path loss and the fading in the vehicular channel several large measurement campaigns [27], [51]–[55] have been performed in a variety of propagation environments such as rural, highway, suburban and urban scenarios. As it is of particular importance to understand how power decays with distance (e.g., from an interference point of view), much effort have been put into finding path loss models, i.e., to characterize the distance dependent power loss. When doing this it has been shown that there is a need to differentiate between line-of-sight (LOS) and non-line-of-sight (NLOS) propagation. For LOS propagation, where the direct path between the Tx and Rx is unobstructed, standard power law models are representative and well accepted [27]:

$$l(\mathbf{x}_\mathrm{tx}, \mathbf{x}_\mathrm{rx}) = A \left\| \mathbf{x}_\mathrm{rx} - \mathbf{x}_\mathrm{tx} \right\|_2^{-\alpha}, \tag{2.2}$$

where $\left\| \mathbf{x}_\mathrm{rx} - \mathbf{x}_\mathrm{tx} \right\|_2$ is the euclidean distance between the Tx and the Rx, α is the path loss exponent, and A is a constant that depends on several factors such as antenna characteristics, carrier frequency, and propagation environment. Note that break point models or two ray models can be used to better adapt to specific scenarios [27]. For NLOS propagation, such as in urban intersection, where buildings block the direct LOS path between vehicles on different roads, measurements on the other hand indicate increased loss over LOS propagation, with complex dependencies on the absolute Tx and Rx locations as well as the width of the roads. Thus a more suitable model for urban intersections is for instance the so-called VirtualSource11p model [54], [55]. However, the complexity of this model renders it intractable when it comes to mathematical analysis. Simpler, and thus more tractable path loss models for urban NLOS communication include the Manhattan model:

$$l(\mathbf{x}_\mathrm{tx}, \mathbf{x}_\mathrm{rx}) = A \left\| \mathbf{x}_\mathrm{rx} - \mathbf{x}_\mathrm{tx} \right\|_1^{-\alpha}, \tag{2.3}$$

which was first proposed in the well-known WINNER II project [56], and the simplified version of the VirtualSource11p model [57]:

$$l(\mathbf{x}_\mathrm{tx}, \mathbf{x}_\mathrm{rx}) = A(\left\| \mathbf{x}_\mathrm{rx} \right\|_2 \left\| \mathbf{x}_\mathrm{tx} \right\|_2)^{-\alpha}, \tag{2.4}$$

where $\left\| \cdot \right\|_1$ is the ℓ_1 norm, and $\left\| \cdot \right\|_2$ is the ℓ_2 norm. Note that both these models assume that the center of the intersection coincides with the origin of the coordinate system, where also the virtual source is placed. Furthermore, the values of α and A might be different from the LOS case. Typical path loss exponents for the vehicular channel are in the ranges of 1.6-2.1 [27], [52]. Note that path loss exponents below 2, i.e., better than free space propagation can be explained by wave-guiding effects, which can be particularly strong in so-called urban canyons. Regarding the fading it has been shown that for LOS links exponential fading is a suitable model [51], [54]. For urban NLOS links on the other hand, a log-normal model with power variations of 3-6 decibels (dB), have been found more appropriate [53]–[55].

2.3 Packet Drops and Random Delays

In this section, we will discuss the underlying causes to why packet drops and random latencies in packet arrivals occur in vehicular networks.[1] We will first consider packet drops, which refers to the inability of the Rx to detect a packet, or the inability to extract the information from a packet. Roughly speaking, a packet can be decoded if the SINR exceeds a certain threshold. The SINR at the Rx can be expressed as

$$\text{SINR} = \frac{P_{\text{t}} g}{\sum_{i \in I} P_{\text{t}} g_i + P_{\text{noise}}}, \tag{2.5}$$

where g is the channel gain between the intended Tx and the Rx, g_i is the channel gain between an interfering Tx and the Rx, P_{t} is the power which each nodes transmits with, and P_{noise} is the noise power due to thermal noise at the Rx. The channel gains g and g_i are random variables, which statistics and autocorrelation depends on a wide variety of factors including the path loss, large-scale fading as well as the fast varying small-scale fading. As mentioned in Section 2.2, the latter effect, which is due to a combination of high vehicle mobility and multipath propagation, can lead to rapidly changing signal propagation conditions and thus drastic changes in the SINR. Hence, one reason for the Rx not being able to decode a packet is that the channel gain g, on the link between the intended Tx and the Rx, is very low. This is referred to as a deep fade. Another reason is that the received interference power is too high. To avoid this, the interference can be controlled through the MAC protocol, but for the ad-hoc network topology enabled by the current standards for V2X, MAC is extremely challenging. For example, the CSMA/CA MAC protocol used in the IEEE 802.11p standard reduces the probability of packet collisions, but the probability still remains non-zero due to reasons such as simultaneous countdown, hidden nodes and same carrier sense time. A brief overview of the basic principles of the CSMA/CA MAC protocol, and some of these effects are given in Fig. 2.2 (for more detailed information regarding the operation of the CSMA/CA MAC protocol used in the IEEE 802.11p standard and the effects mentioned here see e.g., [45]).

Even though the probability of packet collisions is non-zero, the CSMA/CA MAC performs well when there are few users, but in dense scenarios where many users want to send packets over the shared medium the probability of packet collisions (i.e., low SINR), and thus the packet error rate (PER), rapidly increases. The fact that PER rapidly increases with increased vehicle density has also been confirmed by experiments [44].

The main reason for latency in an IEEE 802.11p based network is, as illustrated in Fig. 2.2, the channel access delay, i.e., the random delay until a node gets access to the channel and can transmit its packet. Clearly, the channel access delay is also highly dependent on the channel load, as an increased channel load means more vehicles that

[1] We will not consider multi-hop networks.

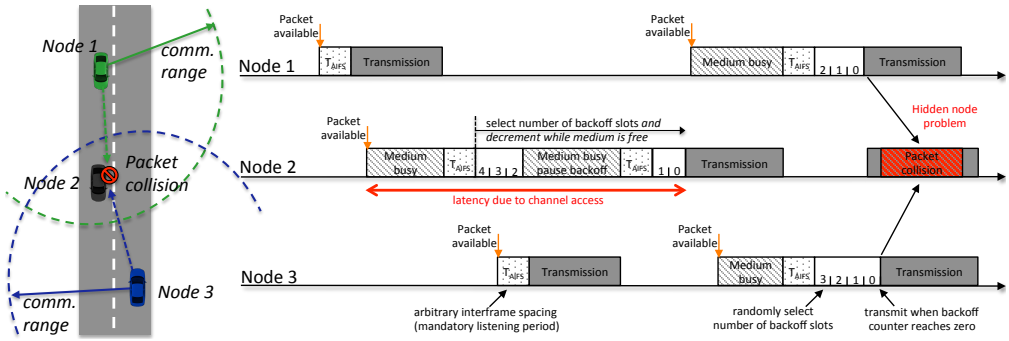

Figure 2.2. Illustration of the mechanisms of the IEEE 802.11p CSMA/CA MAC protocol and how the fact that vehicles have to contend for the shared spectrum leads to packet collisions and unpredictable delays. The figure shows the mandatory listening period before a node can transmit, and how nodes are forced into a back-off procedure if it perceives the medium as busy. Furthermore, it can be seen how packet collisions can occur due to the fact that two nodes that are not within each others sensing range both transmit at the same time, as they both perceive the medium as free. This is referred to as the hidden node problem and does in this case greatly reduce the chances for Node 2 to decode the packets from Node 1 and 3.

contend for the access to the channel.

Based on the above discussion, we see that channel congestion is a major concern in vehicular networks, as the current MAC protocol will results in high PER as well as long channel access delays. However, it should be mentioned that by using so called decentralized congestion control (DCC) methods (which basically operate by either reducing the amount of packets in the network, the transmit power, or the rate) these problems could be made less severe. Hence this is a research topic of special interest. Furthermore, it should be pointed out that other MAC methods for V2X communication have been investigated. In particular, it has been shown that self organizing time division multiple access (STDMA) outperforms CSMA/CA for high network loads as it can provide a bounded and predictable delay [58], [59].

2.4 Challenges for Safety Critical Applications

This section will briefly highlight the main challenges that come with the use of wireless communication techniques in safety critical ITS applications (e.g., cooperative collision avoidance at intersections). First of all these applications typically require extremely low latencies (below 30 ms) and high packet deliver ratios (reliability of 99.999%) for full situational awareness [60], [61]. On top of this relatively long communication ranges (up to 1 km) are desired to be able to plan and increase the time to react in critical

situations. As can be understood it is extremely challenging to be able to guarantee that these requirements are met in the vehicular environment, and thus one of the main challenges is to be able to accommodate for the uncertainties introduced in the system due to latencies and packet drops, preferably by some form of co-design between the control and communication system [23]. In the context of an intersection control system, this could for example be a system that assigns communication resources where it is really needed to keep the channel load low such that low latencies and high packet delivery ratios could be guaranteed. Furthermore, the application need to be able to handle a highly dynamic network with constantly changing network topology, as vehicles due to the high mobility constantly come in and out of communication range, or temporarily disappear due to fades in the channel.

2.5 Stochastic Geometry

In this section, we introduce stochastic geometry, and describe how it can be used to characterize the packet reception probability in a wireless network.

2.5.1 Brief History

Stochastic geometry has roots as far back as to the 18th century and the famous problem of Buffon's needle. However, the development of the stochastic geometry we know today took of with D. G. Kendall, K. Krickeberg and R. E. Miles during the second half of the 20th century [62], and its inherent relation to point process theory and the ability calculate spatial averages has during the years shown to be useful in many different areas, such as biology, material sciences, astronomy and image processing. During the last decade the tools from stochastic geometry have also been extensively used to analyze the impact of interference in wireless networks [63], [64].

2.5.2 Point Processes

A point process is a random process, which for each realization gives rise to a specific point pattern. Hence, point processes are useful tools to model spatial structures in our surrounding, as for example the geographical locations of concurrently transmitting nodes in a wireless network.

Many different types of point processes (e.g., Matérn hard-core processes, Poisson cluster processes) have been used to model the spatial properties of wireless networks, but the simplest and probably most widely used point process is the Poisson point process (PPP). The PPP basically is a spatial generalization of a Poisson process and can be either stationary (homogeneous) or non-stationary (inhomogeneous). The homogeneous PPP can be characterized by a single parameter λ, which describes the constant density of points over space (see Fig. 2.3), and is fully defined by the following two important properties [63]:

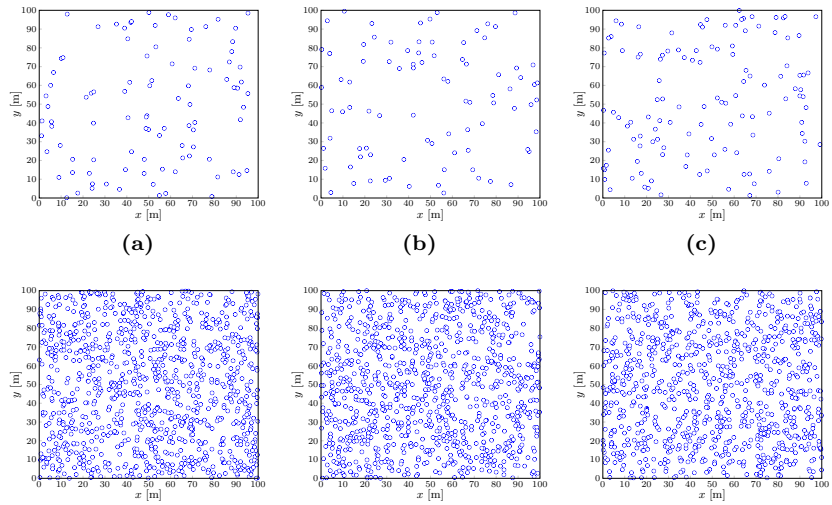

Figure 2.3. Illustrations of homogeneous PPPs in the plane. The upper row,(a)-(c), shows three different realizations of a PPP with density $\lambda = 0.01$, while the bottom row, (d)-(f), shows different realizations of a PPP with density $\lambda = 0.1$.

1. The number of isolated points in any bounded set $B \in \mathbb{R}^n$ is Poisson distributed with mean $\lambda |B|$, where $|B|$ is the Lesbegue measure of B, i.e., the n-dimensional volume.

2. The number of points in disjoint set are independent random variables.

Note that the inhomogeneous PPP is defined in the same way, but by replacing $\lambda |B|$ with $\int_B \lambda(x)\, \mathrm{d}x$, where $\lambda(x)$ is a non-negative function describing the varying density of points over space.

According to the definition, i.e., by using the fact that the number of points in a bounded set follows a Poisson distribution, the probability that a homogeneous PPP has k points in a set B, can be written as

$$\Pr[\Phi(B) = k] = \exp(-\lambda |B|) \frac{(\lambda |B|)^k}{k!}, \tag{2.6}$$

where $\Phi(B)$ denotes the number of points in B. Setting $k = 0$ we also observe that the void probability, i.e., the probability that no points fall within the set B, is given by $\exp(-\lambda |B|)$. Finally, two very interesting and useful properties of the PPP are:

- Superposition of two PPPs with densities λ_1 and λ_2 yields a new PPP with density $\lambda_1 + \lambda_2$

- Thinning of a PPP, i.e., independently selecting points from the original PPP with probability p, results in a new PPP with density λp.

2.5.3 Packet Reception Probability

In this section, we briefly show how stochastic geometry can be used to characterize the packet reception probability for a selected link in a wireless network.

Scenario

We consider a one dimensional network (see Fig. 2.4), with a Tx and Rx located at x_{tx} and x_{rx}, respectively. Furthermore, we assume that the remaining nodes in the network act as interferers and are located according to a homogeneous PPP Φ with density λ, i.e., $\Phi \sim \text{PPP}(\lambda)$. For simplicity, we assume that all nodes except the Rx broadcast

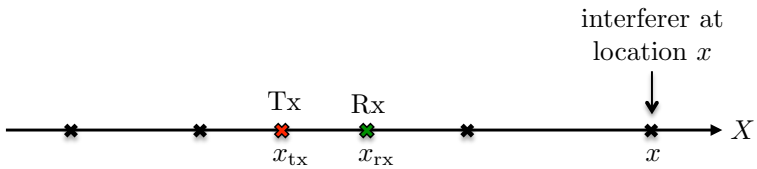

Figure 2.4. Illustration of the one dimensional network.

with a fixed transmission power P_{t}, and that the signal propagation model comprises exponential power fading, i.e. $S \sim \exp(1)$, path loss $l(x_{\text{tx}}, x_{\text{rx}}) = A\,|x_{\text{rx}} - x_{\text{tx}}|^{-\alpha}$, and white Gaussian noise with noise power P_{noise}. Given the setting above, we can express the SINR at the Rx as

$$\text{SINR} = \frac{P_{\text{t}} S_0 l(x_{\text{tx}}, x_{\text{rx}})}{\sum_{x \in \Phi} P_{\text{t}} S_x l(x, x_{\text{rx}}) + P_{\text{noise}}} \tag{2.7}$$

where S_0 represents the fading on the useful link and S_x denotes the fading on an interfering link for an interferer at location $x \in \Phi$. Lastly, we also assume that the only criteria for a packet to be successfully decoded is that the SINR exceeds a threshold β.

Success Probability

Given the scenario outlined above, the probability that the Rx successfully decodes a transmission from the Tx can be expressed as

$$\mathbb{P}(\beta, x_{\text{tx}}, x_{\text{rx}}) = \Pr(\text{SINR} > \beta) \tag{2.8}$$

$$= \Pr\left(\frac{P_{\text{t}} S_0 l(x_{\text{tx}}, x_{\text{rx}})}{I + P_{\text{noise}}} > \beta\right) \tag{2.9}$$

$$= \Pr\left(S_0 > (I + P_{\text{noise}}) \frac{\beta}{P_{\text{t}} l(x_{\text{tx}}, x_{\text{rx}})}\right) \tag{2.10}$$

where

$$I = \sum_{x \in \Phi} P_{\text{t}} S_x l(x, x_{\text{rx}}) \tag{2.11}$$

is the aggregate interference power experienced by the Rx. Conditioned on the path loss we see that the two remaining random variables are the fading on the useful link and the interference power. Hence, to calculate the success probability we need to average over both the fading on the useful link and the interference power (both fading and locations). We start by taking the expectation with respect to the interference, i.e.,

$$\mathbb{P}(\beta, x_{\text{tx}}, x_{\text{rx}}) = \mathbb{E}_I\left\{\Pr\left(S_0 > (I + P_{\text{noise}}) \frac{\beta}{P_{\text{t}} l(x_{\text{tx}}, x_{\text{rx}})}\right)\right\} \tag{2.12}$$

$$= \int_0^\infty \Pr\left(S_0 > (t + P_{\text{noise}})\,\tilde{\beta}\right) f_I(t)\mathrm{d}t \tag{2.13}$$

$$= \int_0^\infty \bar{F}_{S_0}\left((t + P_{\text{noise}})\,\tilde{\beta}\right) f_I(t)\mathrm{d}t \tag{2.14}$$

where $\tilde{\beta} = \frac{\beta}{P_{\text{t}} l(x_{\text{tx}}, x_{\text{rx}})}$ and $\bar{F}_{S_0}(s_0)$ is the complementary cumulative distribution function (CCDF) of the random variable S_0, evaluated in s_0, and $f_I(t)$ denotes the interference distribution. The expression in (2.14) can be interpreted in two ways: (i) as the expectation of $\bar{F}_{S_0}\left((t + P_{\text{noise}})\,\tilde{\beta}\right)$ with respect to the interference distribution; and (ii) the transformation of the interference distribution with a kernel function determined by the CCDF of the fading distribution on the useful link.

Using the fact that the fading in this case is assumed to be exponentially distributed, i.e., has a CCDF of the form

$$\bar{F}_{S_0}(s_0) = e^{-s_0}, \tag{2.15}$$

we can write

$$\mathbb{P}(\beta, x_{\text{tx}}, x_{\text{rx}}) = \int_0^\infty e^{-(t+P_{\text{noise}})\tilde{\beta}} f_I(t)\mathrm{d}t \tag{2.16}$$

$$= e^{-P_{\text{noise}}\tilde{\beta}} \int_0^\infty e^{-t\tilde{\beta}} f_I(t)\mathrm{d}t \tag{2.17}$$

$$= e^{-P_{\text{noise}}\tilde{\beta}} \mathcal{L}_I\left(\tilde{\beta}\right) \tag{2.18}$$

where $\mathcal{L}_I(\cdot)$ denotes the Laplace transform of the interference distribution. The Laplace transform of the interference distribution can also be expressed as

$$\mathcal{L}_I\left(\tilde{\beta}\right) = \mathbb{E}\left[\exp\left(-\tilde{\beta} I\right)\right] \tag{2.19}$$

and substituting (2.11) into (2.19) yields

$$\mathcal{L}_I\left(\tilde{\beta}\right) = \mathbb{E}\left[\prod_{x\in\Phi} \exp\left(-\tilde{\beta}P_{\mathrm{t}}S_x A\left|x-x_{\mathrm{rx}}\right|^{-\alpha}\right)\right] \tag{2.20}$$

$$\overset{(a)}{=} \mathbb{E}_{\Phi}\left[\prod_{x\in\Phi} \mathbb{E}_{S_x}\left\{\exp\left(-\tilde{\beta}P_{\mathrm{t}}S_x A\left|x-x_{\mathrm{rx}}\right|^{-\alpha}\right)\right\}\right] \tag{2.21}$$

$$\overset{(b)}{=} \mathbb{E}_{\Phi}\left[\prod_{x\in\Phi} \frac{1}{1+\tilde{\beta}P_{\mathrm{t}}A\left|x_{\mathrm{rx}}-x_{\mathrm{tx}}\right|^{-\alpha}}\right] \tag{2.22}$$

$$\overset{(c)}{=} \exp\left(-\lambda\int_{-\infty}^{\infty} \frac{1}{1+\left|x-x_{\mathrm{rx}}\right|^{\alpha}/\tilde{\beta}P_{\mathrm{t}}A}\mathrm{d}x\right) \tag{2.23}$$

$$\overset{(d)}{=} \exp\left(-2\lambda\left(\tilde{\beta}P_{\mathrm{t}}A\right)^{1/\alpha}\int_{0}^{\infty} \frac{1}{1+u^{\alpha}}\mathrm{d}u\right) \tag{2.24}$$

$$= \exp\left(-2\lambda\left(\tilde{\beta}P_{\mathrm{t}}A\right)^{1/\alpha}\frac{\pi}{\alpha}\csc\left(\pi/\alpha\right)\right) \tag{2.25}$$

where (a) holds due the independence of the fading parameters, $\mathbb{E}_{\Phi}\left[\cdot\right]$ is the expectation operator with respect to the location of the interferers, and (b) uses the fact that the fading is exponentially distributed. Furthermore, to perform the spatial averaging (c) uses the probability generating functional (PGFL) of a PPP[2] , and (d) involves a variable change $\left|x-x_{\mathrm{rx}}\right|/\left(\tilde{\beta}P_{\mathrm{t}}A\right)^{1/\alpha} \rightarrow u$. For the particular case of $\alpha = 2$, the expression further simplifies to

$$\mathcal{L}_I\left(\tilde{\beta}\right) = \exp\left(-\lambda\sqrt{P_{\mathrm{t}}A\tilde{\beta}}\pi\right). \tag{2.28}$$

Finally, substituting (2.28) into (2.18), and using the variable change $\tilde{\beta} = \frac{\beta\left|x_{\mathrm{rx}}-x_{\mathrm{tx}}\right|^{\alpha}}{P_{\mathrm{t}}A}$, we

[2]The PGFL is a generalization of the probability generating function (PGF), and it completely characterizes a point process. It is defined as [63, Definition A.5]

$$\mathcal{G}[\nu] = \mathbb{E}\prod_{x\in\Phi}\nu(x), \tag{2.26}$$

and as the name implies it is used to calculate the average of a product of a function $\nu(x)\colon \mathbb{R}^d \rightarrow [0,\infty)$ operating on a point process. As in this case, the PGFL is commonly applied when evaluating the Laplace transform of the aggregate interference from a set of nodes distributed according to a point process. The PGFL for a PPP is given by

$$\mathcal{G}[\nu] = \exp\left(-\int_{\mathbb{R}^d}(1-\nu(x))\lambda(\mathrm{dx})\right). \tag{2.27}$$

can for the case of $\alpha = 2$ express the success probability as

$$\mathbb{P}\left(\beta, x_{\text{tx}}, x_{\text{rx}}\right) = \exp\left(-\frac{P_{\text{noise}}\beta\left|x_{\text{rx}} - x_{\text{tx}}\right|^2}{P_{\text{t}}A}\right)\exp\left(-\lambda\sqrt{\beta}\left|x_{\text{rx}} - x_{\text{tx}}\right|\pi\right) \tag{2.29}$$

where the first factor is the success probability in the absence of interferers, and the second factor captures the reduction of the success probability due to interference. In order to illustrate this Fig. 2.5 shows the outage probability, i.e., $\mathbb{P}_{\text{Out}}\left(\beta, x_{\text{tx}}, x_{\text{rx}}\right) = 1 - \mathbb{P}\left(\beta, x_{\text{tx}}, x_{\text{rx}}\right)$, in the interference free case and when the Rx experiences interference from a set of nodes distributed according to a PPP with density $\lambda = 0.001$. Note that we in this scenario have set the transmit power to $P_t = 100$ mW, corresponding to 20 dBm. Furthermore, we have assumed a noise power P_{noise} of -99 dBm, and an SINR threshold of $\beta = 8$ dB [45], and that $A = 0.0025$, approximately matching the conditions in [52].

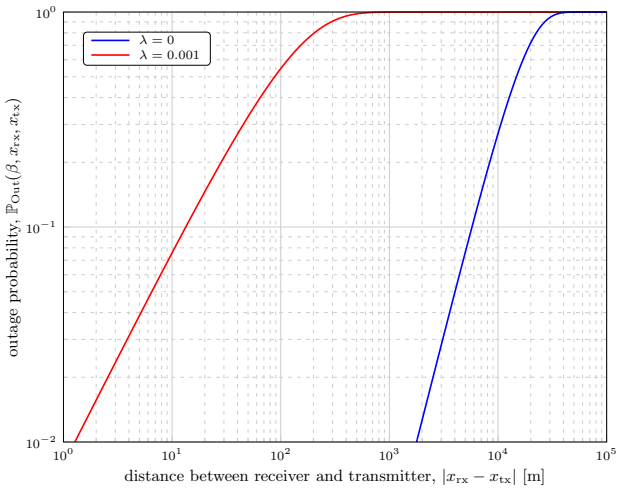

Figure 2.5. Outage probability as a function of the distance between Rx and Tx in the interference free case ($\lambda = 0$) and with interference ($\lambda = 0.001$).

2.6 Summary

In this chapter, we have provided an introduction to vehicular communication and discussed some of the underlaying reasons for packet drops and random latencies. In particular we have learned that interference from other transmitting nodes can severely degraded performance and cause unwanted packet drops. We have also introduced stochastic geometry and showed how it can be used to quantify the effect of interference. In Papers A-D, we use stochastic geometry to analyze the impact of interference in vehicular networks, and to derive analytical key performance metrics on packet reliability and throughput.

CHAPTER 3

Positioning

In this chapter, we give the reader a brief introduction to positioning, and important concepts in this field. Also, we provide an overview of typical positioning requirements and common sensing technologies for ITS. After this, we introduce the concept of Fisher information and Cramér-Rao bounds, and show how these tools can be used to gain insights about the positioning performance in future ITS. Special attention is given to cooperative position solutions, which are foreseen to play an important role when it comes to meeting the demands posed by safety critical ITS applications [30], [34], [36], [65].

3.1 Positioning Basics

3.1.1 Absolute Versus Relative

An important aspect of positioning is in which coordinate system the position information is represented, see Figure 3.1. Typically, one distinguishes between absolute and relative positioning [66], [67]. In absolute positioning, a common frame of reference is used, i.e., agents (e.g. vehicles and other road users with sensing capability) are positioned in a common pre-defined coordinate system. This is typically a reference frame that can be used for navigation. The classical example of an absolute positioning system is GNSS, which uses an earth centered earth fixed reference frame [68].

Relative positioning, on the other hand, focuses on positioning in relation to an agent's or sensor's local environment. In other words, agents are positioned in a local frame, such as a specific vehicle's coordinate system. Even though absolute position information

makes it easier to share information, relative position information can in many cases be sufficient. For example, in most obstacle and collision avoidance applications, it suffices to have an accurate representation of the surrounding environment in the ego vehicle coordinate system. Sensors that provide relative position information include but are not limited to radars, LIDARs and cameras.

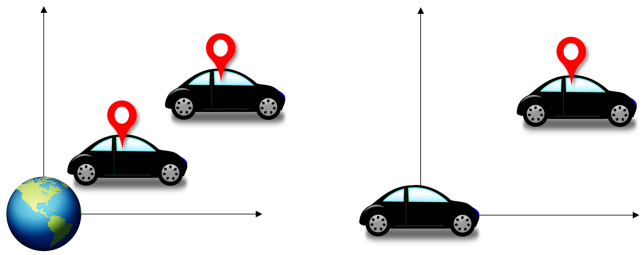

Figure 3.1. Illustration of absolute vs relative positioning.

3.1.2 Noncooperative versus Cooperative

In positioning one can distinguish between noncooperative and cooperative approaches [34], [67], [69]. In noncooperative approaches agents rely solely on their own sensor information for positioning. Cooperative positioning on the other hand, is a multifaceted term that in principle include all approaches where agents in one way or another share measurements providing absolute or relative position information regarding the own or other vehicles position, to improve either the own estimate and view of the environment, or the collective information about the environment.

An important aspect when it comes to cooperative positioning is how measurements are generated and shared. In regards to this, one can differentiate between communication-based and noncommunication-based sensing techniques. Communication-based sensing techniques (e.g., ultra-wideband (UWB) ranging [70]) requires two agents communication to generate measurements, while noncommunication-based sensing techniques (e.g., GNSS, radars, LIDARs and cameras [28], [30], [71], [72]) only requires the involvement of one agent. When it comes to sharing of the data, communication-based sensing techniques typically makes the measurements directly available to the involved agents, while techniques from the second category typically requires a dedicated wireless connection for sharing of the data.

Another important aspect of cooperative positioning is with whom measurements are shared, and how they are used. For instance, one can distinguish between decentralized [67] and centralized [73] approaches. In the decentralized case, each agent have access to either all the measurements, or a subset of measurements (for example from its closest neighbors), and then use this to improve its own position estimate and/or view of where

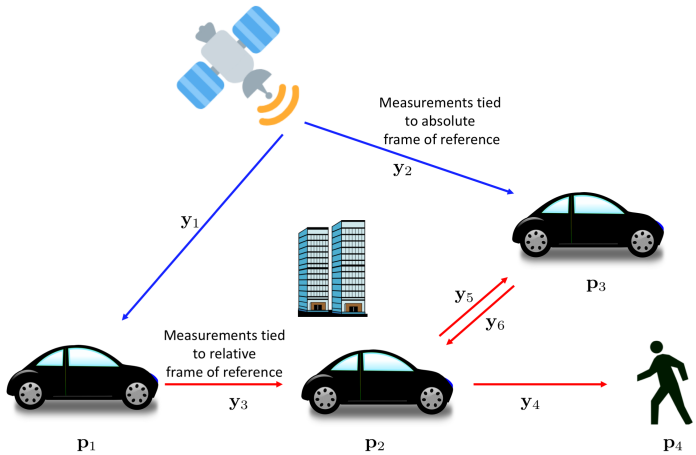

Figure 3.2. Example on cooperative ITS scenario with three vehicles and one pedestrian ($N = 4$ objects) with unknown positions and $M = 6$ measurements. By combining measurements that provide both relative and absolute position information it becomes possible to position objects which if treated alone would be impossible to position in an absolute sense.

everyone else is located. Note that it also can be already processed data that is shared among agents as in [34]. In centralized approaches on the other hand, all measurements are collected at the same place, such as a dedicated agent or cloud server, which estimates everyone's position and creates a map of where everyone is located. Depending on what the use case is this information can then for example either be distributed back to cooperating agents to give them a collective view of the environment, or used as basis for decision in a central controller (e.g., an intersection manager).

3.1.3 The Positioning Problem

The main goal in positioning is to determine the unknown positions of one or several objects in the environment based on observations. These objects can in principle be anything, but in the context of ITS they are typically vehicles, pedestrians or other objects found in the traffic scene, that need to be positioned either in an absolute or relative sense.

To keep it general, we thus let

$$\mathbf{P} = \begin{bmatrix} \mathbf{p}_1^{\mathrm{T}} & \mathbf{p}_2^{\mathrm{T}} & \dots & \mathbf{p}_N^{\mathrm{T}} \end{bmatrix}^{\mathrm{T}} \tag{3.1}$$

denote the unknown positions of N objects. Furthermore, we assume that all the observations that we have at hand, and that in one way or another can be related to the positions $\mathbf{P}$ are aggregated in the measurement vector

$$\mathbf{y} = \begin{bmatrix} \mathbf{y}_1^{\mathrm{T}} & \mathbf{y}_2^{\mathrm{T}} & \dots & \mathbf{y}_M^{\mathrm{T}} \end{bmatrix}^{\mathrm{T}}. \tag{3.2}$$

Formally, the positioning problem, which can be solved using different approaches and algorithms, is then to estimate the vector of unknown positions $\mathbf{P}$ based on the measurement vector $\mathbf{y}$. Commonly, this problem is solved using a statistical model $p(\mathbf{y}|\mathbf{P})$, also referred to as the measurement likelihood. This model describes how the measurements are related to the unknown positions, and characterizes their uncertainties.

The vector $\mathbf{P}$ may vary over time, and its common to apply tracking algorithms to estimate the positions over time. However, in this thesis we focus on snapshots in time, i.e., estimation of the vector $\mathbf{P}$ at given time instances. This can be seen as a subroutine in the tracking problem. Also, we devote most of our attention to cooperative positioning scenarios in the context of ITS, an example of such a scenario is illustrated in Figure 3.2.

3.1.4 Estimators

Estimators play an important role in solving the positioning problem. Typically, one distinguishes between non-Bayesian and Bayesian estimators. Estimators belonging to the first category treats the unknown quantity as deterministic but unknown, while Bayesian estimators considers the unknown quantity to be random. An example of a well known estimator from the non-Bayesian category is the maximum likelihood (ML) estimator, defined as [67], [74]:

$$\hat{\mathbf{P}}_{\mathrm{ML}} = \arg\max_{\mathbf{P}} p(\mathbf{y}|\mathbf{P}), \tag{3.3}$$

where $p(\mathbf{y}|\mathbf{P})$ is the likelihood of the measurements. In the Bayesian case the unknown quantity, in this case the positions, is regarded as a random vector with a priori distribution $p(\mathbf{P})$. An example on a well known estimator in this category is the maximum a posteriori (MAP) estimator, defined as [67], [74]:

$$\hat{\mathbf{P}}_{\mathrm{MAP}} = \arg\max_{\mathbf{P}} p(\mathbf{P}|\mathbf{y}), \tag{3.4}$$

where $p(\mathbf{P}|\mathbf{y})$ is the posterior distribution. While the ML estimate $\hat{\mathbf{P}}_{\mathrm{ML}}$ maximizes the likelihood of the measurements, the MAP estimate $\hat{\mathbf{P}}_{\mathrm{MAP}}$ correspond to the mode of the posterior distribution, i.e., the most likely position vector given both the measurements and the a priori information $p(\mathbf{P})$. Other estimators often used in the positioning context are the least squares (LS) estimator and the minimum mean square error (MMSE) estimator.

In a cooperative ITS scenario, ML involves solving a high-dimensional nonlinear optimization problem. To gain insight on the solution, without explicitly solving the ML problem, one can revert to fundamental performance bounds, which will be covered in Section 3.4 and Section 3.5.

3.2 Positioning Requirements

Cooperative ITS will enable a wide range of applications, including everything from simple applications that increases the awareness of the driver (such as road works warning and emergency electronic braking [75]), to more transformational applications such as cooperative automated driving, where vehicles are explicitly coordinated and controlled to optimize the traffic flow. According to the Car-2-Car Communication Consortium (C2C-CC) roadmap, the deployment of these different applications is envisioned to be stage wise and occur in phases, see Figure 3.3.

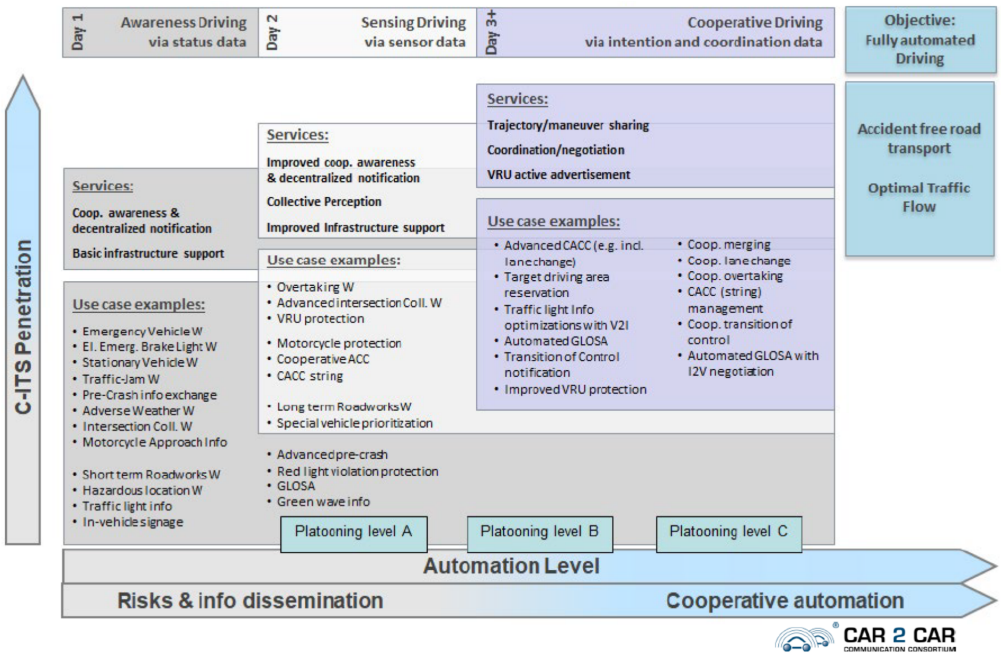

Figure 3.3. The C2C-CC roadmap on services and example use cases (used with permission from C2C-CC).

Understandably, the applications in the various phases (i.e., Day 1 to Day 3 and beyond) poses different requirements in terms of positioning. For application that focuses on increasing the awareness of the driver (i.e., Day 1), the requirements are less stringent. Typically one say that its sufficient with road-level positioning, i.e., one to a few meters positioning accuracy. As the level of automation increased the positioning requirements typically become more stringent, as it now also becomes important to know both in which lane and where in the lane the vehicle is positioned. For safety critical applications, such as cooperative automated driving (i.e, Day 3 and beyond), one often talk about positioning requirements of a few tens of centimeters. In Table 3.1, we list a few applications

Application/Use case	accuracy requirement	automation level
Road works warning	>1 m	low
See through vehicle	>1 m	low
Bird's eye view	>1 m	low
Vulnerable road user discovery/protection	10-50 cm	low
Platooning	10-30 cm	high
Automated overtake	10-30 cm	high
Cooperative Collision avoidance	10-30 cm	high

Table 3.1. Positioning requirements for cooperative ITS applications (based on [32], [60], [61], [76]).

and their associated positioning requirements. Note that the requirements presented in Table 3.1 are based on everything from simulations to expert opinions, and are intended to provide an indication of the required order of magnitude rather than an exact value.

3.3 Common Sensing Technologies

Positioning in a complex traffic environment is an intricate problem, and there is no single sensing technology that alone can meet the demands on accuracy and reliability posed by safety critical ITS applications, especially if considering that it should work both night and day as well in all types of weather conditions. Thus, future vehicles are expected to rely on a combination of sensors and information sources for positioning of the own vehicle as well as other objects in the surrounding [67], [71]. These include for example, GNSS, radar, laser scanners (LIDAR), mono and stereo cameras, ultrasonic sensors. The latter sensors are all typical examples on what is often referred to as relative position sensors, while the signals received from GNSS satellites can be used to compute the vehicles absolute position in a known reference frame. Typically, vehicles are also equipped with inertial sensors (i.e., IMUs), which can be used for dead reckoning.[1] In addition to the traditional sensors, future automated vehicles will also use HD map information, which if combined with sensor data from relative position sensors can be used to position the vehicle in an absolute sense. As vehicles are foreseen to be connected to both each other and the cloud (using both ITS G5 and cellular), it is also expected that a vital source of information in future ITS will be cooperative sensor data, i.e., sensor data received from nearby vehicles or infrastructure. Furthermore, it has been shown that future 5G cellular exhibits properties that can make it a great positioning source, and it is therefore not unlikely that 5G based positioning become an important part in the positioning puzzle for future ITS [67]. An overview of the main sensor technologies and information sources

[1] keeping track of the position based on information about the traveled time, direction and speed

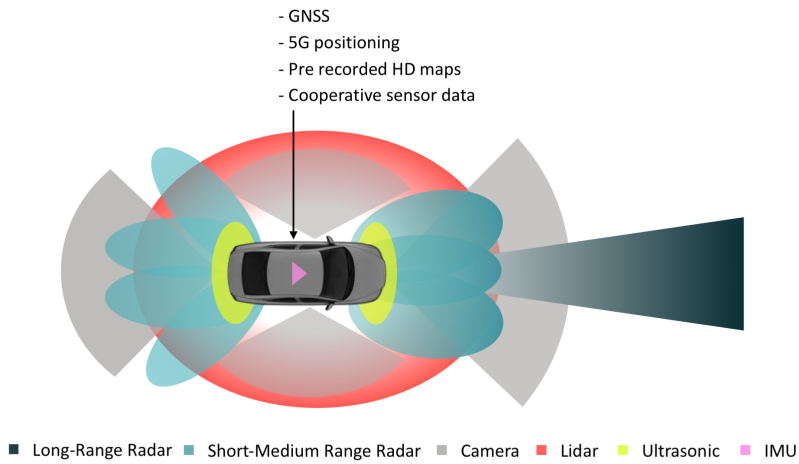

Figure 3.4. Overview of main ITS sensor technologies and information sources.

related to vehicular positioning is given in Figure. 3.4. Below we give a brief introduction to a selection of these and discuss their properties from a vehicular perspective.

3.3.1 GNSS

Satellite bases position is today one of the most widespread positioning technologies, and global navigation satellite systems (GNSS) receivers can be found in anything from mobile phones to space shuttles. Formally, the name GNSS is the generic term for a satellite based positing system with global coverage. This includes for example the well known American system GPS, the Russian system GLONASS as well as the European system Galileo. All these systems have their own constellation of satellites orbiting the earth, which work together with a network of ground stations, and transmits coded radio frequency signals in the L-band at precise time intervals. Observations of these signals can then be used to obtain range estimates between the satellites and a GNSS receiver, and through knowing the location of the satellites and having observations from at least four satellites it is then possible for the user to pin-point its position on earth. The accuracy in the obtained position depends on which positioning technique that is used. The three main approaches are:

- **Code-based positioning:** This method relies on observations of the code phase of the transmitted signals for estimation of the ranges to the satellites. This technique typically gives an accuracy of one to a few meters [71], [77] and is the technique used in low-cost mass market receivers.
- **Real Time Kinematic (RTK):** RTK is a relative positioning method, which relies on observations of the carrier phase for more accurate range estimation, and

uses information form a nearby reference station with known location to cancel out common error sources. RTK provides centimeter level positioning [71], [77]. Compared to code-based positioning it is less robust. Mainly due to the less robust carrier tracking, and the fact that if the receiver temporary loses track of the carrier phase it needs to reinitialize and again go through the involved process of ambiguity resolution, which deals with determining the unknown number of carrier cycles between the satellite and the receiver. Typical applications include land surveying and machine guidance at construction sites

- **Precise Point Positioning (PPP):** PPP is a method that makes it possible to achieve decimeter level accuracies with a single GNSS receiver. Just like RTK, it utilizes the precise carrier phase observation. However, instead of relying on data from a nearby reference station, it utilizes advanced models and corrections generated from a global network of reference stations. This makes PPP suitable for applications in areas where there is no fixed infrastructure in the vicinity. One major downside with PPP is its long convergence times. Typically, it can take 20 to 40 minutes to reach an accuracy of 10 cm [77].

A more in-depth description of how GNSS works and the different methods can be found in, for example, [68], [77].

When it comes to automotive applications GNSS is already extensively used, as more or less all vehicles equipped with a navigation system has some form of low-cost receiver for code-based positioning. On the other hand, RTK or PPP solutions are despite their astonishing precision, still not seen as viable options on the commercial vehicle side [78]. Some of the common explanations for this are [78], [79]: 1) the receivers are still relatively expensive; 2) the positioning is not deemed robust enough; 3) initialization times are too long; 3) reference data is not available for mass market applications on a regional or global scale. Though, it should be pointed out, that RTK has since long been the de facto standard for positioning when it comes to testing and evaluation automated driving systems and advanced driver support systems. In connection to this, it should also, be mentioned that there are ongoing initiatives that focus on making correction data, and thus high precision GNSS, available for mass market applications. For instance, SAPCORDA (which is a joint venture by Bosch, Geo++, Mitsubishi Electric and u-blox) and the Swedish project Network-RTK Positioning for Automated Driving (NPAD).

On a more general level it can be mentioned that the main advantages and reasons for using GNSS as a sensor in future automotive applications are that it has global coverage and is a source of absolute positioning information, i.e., the position is provided in a global frame of reference. Some of the downsides with GNSS, are that it more or less relies on line of sight (LOS) reception of the signals, which can be particularly challenging in urban canyons and tunnels. Moreover, GNSS signals are relatively easy to jam or spoof.

Simple GNSS model

GNSS measurements can be modeled in many different ways depending on the level of abstraction and detail. For instance, one can consider range measurements to individual satellites (so called pseudoranges) or processed measurements with respect to at last four satellites, leading to a position. Taking a high-level perspective, we model GNSS measurements that agent i make as noisy observations of its absolute position $\mathbf{p}_i$, i.e., [28]:

$$\mathbf{y}_{ii}^{\mathrm{G}} = \mathbf{p}_i + \mathbf{n}_{ii}^{\mathrm{G}}, \tag{3.5}$$

where $\mathbf{n}_i^{\mathrm{G}} \sim \mathcal{N}(0, \mathbf{\Sigma}_{ii})$ is zero mean Gaussian measurement noise with covariance $\mathbf{\Sigma}_{ii} = \sigma_{G,i}^2 \mathbf{I}_2$.

3.3.2 Radar

The term radar, which stands for radio detection and ranging, was coined by the US military in the 1940s. The basic principle behind radar technology is to emit known electromagnetic signals, and then analyze the part of the signal that is reflected back. By doing this it is possible to detect and identify objects in the surrounding environment. Information that can be retrieved from a radar sensor includes the range and bearing to the detected object, which basically correspond to the relative position of the detected object in the radar coordinate system. By exploiting the Doppler effect it is typically also possible to obtain the relative speed of the object. For a comprehensive description and background on radar technology see, e.g., [80].

When it comes to the automotive sector, radars sensor are already today used in advanced driver support systems such as forwards collision warning systems, adaptive cruise control, lane change assistance. Automotive radars typically work in either the 24 GHz band or the 79 GHz band. Benefits with the latter band includes better resolution and Doppler sensitivity as well as smaller sensors dimensions [71]. The two main radar technologies for ITS are:

- **Impulse radars,** which in the classical sense emits short pulses and then measures the time it takes for the pulse to travel to the object and back.
- **Frequency-Modulated Continuous Wave (FMCW) radars**, which emit frequency chirped signals with constant power envelope. The range to the object is in this case derived by using that the distance to the object is proportional to the frequency difference between the outgoing and incoming reflected signal.

For automotive radars one also distinguishes between short-range radar, medium-range radar and long-range radar. Long range radars can have a perception range up to 250 m, and commonly a narrower field of view (FOV). Typical range accuracies are from 10 cm up to 5% of the measured range, and the angular resolution that can be obtained lies between 0.5° and 5°[71].

Some of the advantages with using radars for automotive applications are their relatively long range compared to other sensors, as well as their insensitivity to surrounding light and weather conditions.

Simple Radar Model

Given a high level of abstraction, we can similarly as in [28], [29], model radar observations that agent i makes of agent j as relative positions in vehicle i's local coordinate frame, i.e.,

$$\mathbf{y}_{ij}^{\mathrm{R}} = \mathbf{R}(\psi_i)(\mathbf{p}_j - \mathbf{p}_i) + \mathbf{n}_{ij}^{\mathrm{R}}, \tag{3.6}$$

where

$$\mathbf{n}_{ij}^{\mathrm{R}} \sim \mathcal{N}(0, \mathbf{\Sigma}_{ij}) \tag{3.7}$$

and

$$\mathbf{R}(\psi_i) = \begin{bmatrix} \cos(\psi_i) & \sin(\psi_i) \\ -\sin(\psi_i) & \cos(\psi_i) \end{bmatrix} \tag{3.8}$$

is ψ_i is the heading of agent i (and the radar), and $\mathbf{R}(\psi_i)$ is the rotation matrix between the global coordinate frame and the local frame. Since radars typically make mutually independent measurements in range (r) and bearing (α) in a polar coordinate system, the noise components are not independent in the local cartesian frame. We approximate the covariance of the radar measurement noise in the local cartesian frame as

$$\mathbf{\Sigma}_{ij} = \mathbf{R}^{\mathrm{T}}(\alpha_{ij})\mathbf{\Sigma}_{ij}^{\mathrm{P}^*}\mathbf{R}(\alpha_{ij}) \tag{3.9}$$

where

$$\mathbf{\Sigma}_{ij}^{\mathrm{P}^*} = \begin{bmatrix} \sigma_{r,i}^2 & 0 \\ 0 & (r_{ij}\sigma_{\alpha,i})^2 \end{bmatrix} \tag{3.10}$$

is an approximation of the covariance in a cartesian coordinate system $\{\mathrm{P}^*\}$ aligned with the radial and angular axis of the original polar coordinate system. Furthermore, $\sigma_{r,i}$ and $\sigma_{\alpha,i}$ are the standard deviations of the mutually independent noise components of the range and bearing measurements in the original polar coordinate system, and r_{ij} and α_{ij} are the range and bearing between vehicle i and j, respectively. Furthermore, we assume that the sensor field of view (FOV) is determined by an opening angle θ_{FOV} and a maximum detection range $r_{\max}$.

A remark in relation to this is that in radar sensing there is generally no knowledge about the ID of agent j. This is typical for noncommunication-based sensing technologies and leads to the need to perform a data association step in order to relate measurements to objects. Such data association is a research topic by itself and not considered in this thesis. In general, when objects are sufficiently well separated and there is little clutter, the assumption of a known data association is reasonable.

3.3.3 LIDAR

The LIDAR (light detection and ranging) technology originates from the 1960, and has since then been used in a wide range of fields, for example geology, archeology, forestry, atmospheric studies and laser altimetry. Conceptually, LIDAR sensors, sometimes also referred to as laser scanners, work in the same way as radars, but in the optical part of the spectrum. By emitting laser beams and analyzing the backscattered light it is possible to detect and compute the distance to an object. The possibility to collimate laser light in combinations with the short wavelength provides fantastic spatial resolution and accuracy, and by steering the laser beam in different directions it is possible to build up a 3D like representation of the environment. Automotive LIDARs work in the near infrared region, and the perception range, which strongly depends on the reflectivity of the object is typically between 80 m and 200 m [71]. Furthermore, typical range accuracies are between 0.02 m and 0.5 m, and angular resolution is about 0.1°. Also, one typically distinguishes between mechanical and solid-state LIDARs:

- **Mechanical LIDARs**, were the type of LIDARs used in many of the early self-driving car projects (e.g. Google's self-driving car in 2009). These use a mechanically rotating assembly in combination with high grade optics to steer the laser beam and scan the environment. These radars are typically bulky but provide high SNR and wide FOV.

- **Solid-state LIDARs**, are the result of recent advances in technology, and has made it possible to significantly shrink LIDAR sensor. They rely on a few different underlying principles and thus implementation methods. These include MEMS LIDARs, which uses tiny mirrors that are electromechanically steered; Flash LIDARs, which simply put works similarly to a digital camera by illuminating the environment in front of it; Optical phase array (OPA) LIDARs, which works similar to a phase steered radars.

For a more detailed description of the different LIDAR technologies see [81].

The main reason for using LIDARs as an automotive sensor is that they provide an incredibly detailed and accurate description of the environment, which for example is very useful when it comes to obstacle detection and collision mitigation. Furthermore, the accurate information from the LIDAR, has the potential to play a vital role when positioning the vehicle in relation to other objects. Some limitations with LIDARs (in contrast to radars) are that they have difficulties in detecting objects at close distances, and that their performance degrades in weather conditions such as rain, snow and fog. Also, LIDARs are susceptible to ambient light conditions. For instance, incident sunlight in the morning and afternoon can give rise to disturbances [71].

From a high-level perspective, LIDAR measurements can be modeled in the same way as radar measurements, i.e., as relative positions in the local coordinate frame.

3.4 Fisher Information and the Cramér-Rao Bound

In this section, we review the concepts of Fisher information and Cramér-Rao bounds.

3.4.1 FIM Fundamentals

The Cramér-Rao lower bound (CRLB), which was derived by Harald Cramér and Calyampudi Radhakrishna Rao in the 1940s, expresses a bound on the variance of any unbiased estimator of deterministic but unknown parameters and can be used to obtain insights about the quality of estimation algorithms. The CRLB is derived from the Fisher Information Matrix (FIM), which given a statistical measurement model describes the information that the observations carry about the unknown parameters. If we let $\boldsymbol{\theta} = [\boldsymbol{\theta}_1^{\mathrm{T}} \dots \boldsymbol{\theta}_K^{\mathrm{T}}]^{\mathrm{T}}$ represent the vector of unknown parameters that we want to estimate, and $\mathbf{y}$ the vector of measurements or observables, which are described by the statistical model $p(\mathbf{y}|\boldsymbol{\theta})$, we can express the FIM as [74]

$$\mathbf{J}(\boldsymbol{\theta}) = -\mathbb{E}_{\mathbf{y}} \left\{ \nabla_{\boldsymbol{\theta}}^{\mathrm{T}} \nabla_{\boldsymbol{\theta}} \log p(\mathbf{y}|\boldsymbol{\theta}) \right\}, \tag{3.11}$$

where $\mathbb{E}\{\cdot\}$ denote the expectation operator and ∇_θ is the gradient operator with respect to the parameter vector $\boldsymbol{\theta}$. Note that a requirement for the FIM to be computable is that the log-likelihood function, i.e., $\log p(\mathbf{y}|\boldsymbol{\theta})$, is twice differentiable and that a few regularity conditions hold [82]. To provide some intuition regarding the expression in (3.11) it can be seen that $\mathbf{J}(\boldsymbol{\theta})$ correspond to the expected curvature of the log-likelihood function. Loosely speaking, this means that the "sharper" the log-likelihood function is the more information the observations carry about the parameters that we want to estimate. While the expression in (3.11) is valid for any measurement likelihood for which the previously discussed conditions hold, we can for the not so uncommon assumption of additive Gaussian observation noise, i.e., $\mathbf{y} \sim \mathcal{N}(\mathbf{f}(\boldsymbol{\theta}), \Sigma(\boldsymbol{\theta}))$, and when the covariance is independent of $\boldsymbol{\theta}$, i.e., $\boldsymbol{\Sigma}(\boldsymbol{\theta}) = \boldsymbol{\Sigma}$, simply write the FIM as [74]

$$\mathbf{J}(\boldsymbol{\theta}) = \nabla_{\boldsymbol{\theta}}^{\mathrm{T}} \mathbf{f}(\boldsymbol{\theta}) \boldsymbol{\Sigma}^{-1} \nabla_{\boldsymbol{\theta}} \mathbf{f}(\boldsymbol{\theta}), \tag{3.12}$$

Important properties pertaining to the FIM $\mathbf{J}(\boldsymbol{\theta})$ are:

- It is a positive semi-definite matrix, i.e., $\mathbf{J}(\boldsymbol{\theta}) \succeq 0$
- Information from independent observations add up, i.e., if $\mathbf{J}^{\mathbf{y}_1}(\boldsymbol{\theta})$ and $\mathbf{J}^{\mathbf{y}_2}(\boldsymbol{\theta})$ represent the Fisher information from the independent observations $\mathbf{y}_1$ and $\mathbf{y}_2$, the total information from these observation is $\mathbf{J}(\boldsymbol{\theta}) = \mathbf{J}^{\mathbf{y}_1}(\boldsymbol{\theta}) + \mathbf{J}^{\mathbf{y}_2}(\boldsymbol{\theta})$

Given the FIM $\mathbf{J}(\boldsymbol{\theta})$, which depending on the setting can be computed by either (3.11) or (3.12), the CRLB on the covariance of an unbiased estimator $\hat{\boldsymbol{\theta}}$ is now simply $\mathbf{J}^{-1}(\boldsymbol{\theta})$, i.e., [74]

$$\mathbf{J}^{-1}(\boldsymbol{\theta}) \preceq \mathbb{E}_{\mathbf{y}} \left\{ (\boldsymbol{\theta} - \hat{\boldsymbol{\theta}})(\boldsymbol{\theta} - \hat{\boldsymbol{\theta}})^{\mathrm{T}} \right\}. \tag{3.13}$$

In other words, the inverse of the FIM provides a lower bound on the theoretically achievable estimation accuracy, and intuitively this reciprocal relationship implies that the more information we have the better we should be able to estimate the unknown parameters. As a final remark, it should be mentioned that an advantage with the CRLB is that it can be computed without having to consider a specific estimation method or specific measurements, the only thing that is required is a statistical model for the observations on the form $p(\mathbf{y}|\boldsymbol{\theta})$.

3.4.2 Equivalent Fisher Information

It is not uncommon that the parameter vector $\boldsymbol{\theta}$ is high dimensional and includes nuisance parameters, i.e., parameters that are not of immediate interest but can not be left out of the analysis. The equivalent Fisher information matrix (EFIM) is a tool to reduce the dimensionality of the problem and extract the information corresponding to the subset of parameters that we are interested in. More precisely, given a parameter vector $\boldsymbol{\theta} = \begin{bmatrix}\boldsymbol{\theta}_1^{\mathrm{T}} & \boldsymbol{\theta}_2^{\mathrm{T}}\end{bmatrix}^{\mathrm{T}}$, with corresponding FIM

$$\mathbf{J}(\boldsymbol{\theta}) = \begin{bmatrix}\mathbf{A} & \mathbf{B} \\ \mathbf{B}^{\mathrm{T}} & \mathbf{C}\end{bmatrix} \tag{3.14}$$

where $\boldsymbol{\theta}_1 \in \mathbb{R}^m$, $\boldsymbol{\theta}_2 \in \mathbb{R}^n$,$\mathbf{A} \in \mathbb{R}^{m\times m}$, $\mathbf{B} \in \mathbb{R}^{m\times n}$ and $\mathbf{C} \in \mathbb{R}^{n\times n}$, the EFIM corresponding to $\boldsymbol{\theta}_1$ is defined as [31]

$$\mathbf{J}_{\mathrm{e}}(\boldsymbol{\theta}_1) = \mathbf{A} - \mathbf{B}\mathbf{C}^{-1}\mathbf{B}^{\mathrm{T}}, \tag{3.15}$$

where the right hand side in (3.15) is known as the Schur complement of the matrix $\mathbf{C}$. The EFIM $\mathbf{J}_{\mathrm{e}}(\boldsymbol{\theta}_1)$, which is a matrix of size $m \times m$, retains all information regarding the unknown parameters $\boldsymbol{\theta}_1$ in the sense that $\mathbf{J}_{\mathrm{e}}^{-1}(\boldsymbol{\theta}_1)$ correspond to the CRLB on $\boldsymbol{\theta}_1$. This property has shown to be very useful, in particular as it alleviates computational complexity by providing a way to reduce the dimensionality of the problem and computing the CRLB on individual parameters without having to invert the complete FIM $\mathbf{J}(\boldsymbol{\theta})$. The fact that the EFIM can be used to extract the information pertaining to certain parameters can also be used to provide insights on how different observations would contribute in estimating the parameter in question.

3.4.3 Position Error Bound

When comparing bounds on different agents position it can be useful to have scalar measure in addition to the obtained CRLBs, which most often are on matrix form due to the multi-dimensional nature of the positions. One such measure, which is directly based on the CRLB, is the position error bound (PEB). Given an agent i with position $\mathbf{p}_i$, and its corresponding CRLB $\mathbf{J}_{\mathrm{e}}^{-1}(\mathbf{p}_i)$, the PEB is expressed in meters and is defined

as [31]

$$\mathcal{P}(\mathbf{p}_i) = \sqrt{\mathrm{tr}\left\{\mathbf{J}_{\mathrm{e}}^{-1}(\mathbf{p}_i)\right\}}, \tag{3.16}$$

where $\mathrm{tr}\{\cdot\}$ denotes the trace operator.

3.5 Bounds on Cooperative Positioning in ITS

In this section, we will show how the tools introduced in Section 3.4, can be used to evaluate the expected positioning performance in a vehicular scenario like the one in Paper G. We will start by a general description of the type of scenario that we are interested in, and then show how to derive position error bounds for a small toy example with three vehicles.

3.5.1 General System Model

Consider a cooperative heterogeneous traffic scenario, consisting of N vehicles with varying sensing and communication capabilities. Vehicles with sensors are assumed to be able to send their observations to a central server (e.g. a road side unit or dedicated vehicle), with aim to position the N vehicles. Vehicles are modeled as point objects, and we denote the unknown sate of vehicle i by $\mathbf{x}_i$, comprising the position $\mathbf{p}_i \in \mathbb{R}^2$ and heading $\psi_i \in \mathbb{R}^1$. Moreover, we assume that a vehicle is equipped with a combination of (i) a GNSS module for observing its own position; (ii) a radar for observing other vehicles; (iii) a compass for observing its heading. Observations from the sensor are assumed to be on the general form

$$\mathbf{y}_{ij} = \mathbf{f}(\mathbf{x}_i, \mathbf{x}_j) + \mathbf{n}_{ij}. \tag{3.17}$$

where $\mathbf{f}(\cdot)$ is a function dependent on the state of the involved vehicles, which in this case is vehicle i and j, and $\mathbf{n}_{ij}$ is measurement noise. For GNSS and radar observations, we use the models presented in Section 3.3.1 and Section 3.3.2, i.e., observations have the form

$$\mathbf{y}_{ii}^{\mathrm{G}} = \mathbf{f}_{ii}^{\mathrm{G}}(\mathbf{x}_i, \mathbf{x}_i) + \mathbf{n}_{ii}^{\mathrm{G}} = \mathbf{p}_i + \mathbf{n}_{ii}^{\mathrm{G}} \tag{3.18}$$

and

$$\mathbf{y}_{ij}^{\mathrm{R}} = \mathbf{f}_{ij}^{\mathrm{R}}(\mathbf{x}_i, \mathbf{x}_j) + \mathbf{n}_{ij}^{\mathrm{R}} = \mathbf{R}(\psi_i)(\mathbf{p}_j - \mathbf{p}_i) + \mathbf{n}_{ij}^{\mathrm{R}}. \tag{3.19}$$

Compass observations made by vehicle i are modeled as [28]

$$\mathbf{y}_{ii}^{\mathrm{C}} = \mathbf{f}_{ii}^{\mathrm{C}}(\mathbf{x}_i, \mathbf{x}_i) + n_{ii}^{\mathrm{C}} = \psi_i + n_{ii}^{\mathrm{C}} \tag{3.20}$$

where $n_{ii}^{\mathrm{C}} \sim \mathcal{N}\left(0, \sigma_{\mathrm{C},i}^2\right)$.

3.5.2 Three Vehicle Toy Example

Let us now consider the $N = 3$ vehicles case illustrated in Figure. 3.5. The first vehicle

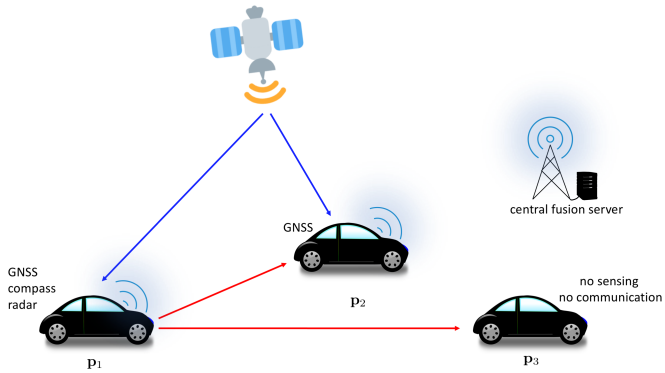

Figure 3.5. Illustration of three vehicle scenario. Vehicles have different sensing capabilities. Blue arrows represent GNSS measurements that provide absolute position information, and red arrows represent radar measurements that provide relative position information

$(i = 1)$, is fitted with a GNSS receiver, a compass, and a radar. The second vehicle $(i = 2)$ is equipped with a GNSS receiver, and the third vehicle $(i = 3)$ has no sensors (or no communication). Furthermore, we assume that second and third vehicle are in the FOV of the first vehicle's radar, which is illustrated by the red arrows in Figure. 3.5.

Basic FIM Analysis

Given this scenario and the system model from Section 3.5.1, we can then write the vector of unknown parameters as

$$\boldsymbol{\theta} = \begin{bmatrix} \mathbf{p}_1^{\mathrm{T}} & \mathbf{p}_2^{\mathrm{T}} & \mathbf{p}_3^{\mathrm{T}} & \psi_1 & \psi_2 & \psi_3 \end{bmatrix}^{\mathrm{T}}. \tag{3.21}$$

i.e., the three vehicle positions $\mathbf{p}_1$ to $\mathbf{p}_3$, and the three vehicle headings ψ_1 to ψ_3. Furthermore, we can write the measurement vector as

$$\mathbf{y} = \begin{bmatrix} [\mathbf{y}_{11}^{\mathrm{G}}]^{\mathrm{T}} & [\mathbf{y}_{11}^{\mathrm{C}}]^{\mathrm{T}} & [\mathbf{y}_{12}^{\mathrm{R}}]^{\mathrm{T}} & [\mathbf{y}_{13}^{\mathrm{R}}]^{\mathrm{T}} & [\mathbf{y}_{22}^{\mathrm{G}}]^{\mathrm{T}} \end{bmatrix}^{\mathrm{T}}. \tag{3.22}$$

Given the additive Gaussian nature of the observation noise, we can then express the joint measurement likelihood as

$$p(\mathbf{y}|\boldsymbol{\theta}) = \mathcal{N}\left(\mathbf{f}(\boldsymbol{\theta}), \boldsymbol{\Sigma}\right) \tag{3.23}$$

where

$$\mathbf{f}(\boldsymbol{\theta}) = \begin{bmatrix} [\mathbf{f}_{11}^{\mathrm{G}}(\mathbf{x}_1, \mathbf{x}_1)]^{\mathrm{T}} & [\mathbf{f}_{11}^{\mathrm{C}}(\mathbf{x}_1, \mathbf{x}_1)]^{\mathrm{T}} & [\mathbf{f}_{12}^{\mathrm{R}}(\mathbf{x}_1, \mathbf{x}_2)]^{\mathrm{T}} & [\mathbf{f}_{13}^{\mathrm{R}}(\mathbf{x}_1, \mathbf{x}_3)]^{\mathrm{T}} & [\mathbf{f}_{22}^{\mathrm{G}}(\mathbf{x}_2, \mathbf{x}_2)]^{\mathrm{T}} \end{bmatrix}^{\mathrm{T}} \tag{3.24}$$

and the block diagonal matrix

$$\boldsymbol{\Sigma} = \begin{bmatrix} \boldsymbol{\Sigma}_{11} & & & & & \\ & \sigma^2_{\mathrm{C},1} & & & & \\ & & \boldsymbol{\Sigma}_{12} & & & \\ & & & \boldsymbol{\Sigma}_{13} & & \\ & & & & \boldsymbol{\Sigma}_{22} \end{bmatrix}. \tag{3.25}$$

According to (3.12), the FIM $\mathbf{J}(\boldsymbol{\theta})$ is then given by

$$\mathbf{J}(\boldsymbol{\theta}) = \nabla^{\mathrm{T}}_{\boldsymbol{\theta}} \mathbf{f}(\boldsymbol{\theta}) \boldsymbol{\Sigma}^{-1} \nabla_{\boldsymbol{\theta}} \mathbf{f}(\boldsymbol{\theta}). \tag{3.26}$$

In other words, to evaluate the FIM $\mathbf{J}(\boldsymbol{\theta})$, we first need to determine the inverse of the covariance matrix $\boldsymbol{\Sigma}^{-1}$ as well as the Jacobian matrix $\nabla_{\boldsymbol{\theta}} \mathbf{f}(\boldsymbol{\theta})$. The inverse covariance matrix $\boldsymbol{\Sigma}^{-1}$ is simply obtained by taking the inverse of each diagonal block. To determine the Jacobian $\nabla_{\boldsymbol{\theta}} \mathbf{f}(\boldsymbol{\theta})$, we first conclude that the only non-zero derivatives that we have to take into account are of the form

$$\frac{\partial \mathbf{f}^{\mathrm{G}}_{ii}(\mathbf{x}_i, \mathbf{x}_i)}{\partial \mathbf{p}_i} = \frac{\partial \mathbf{p}_i}{\partial \mathbf{p}_i} = \mathbf{I}_2 \tag{3.27}$$

$$\frac{\partial \mathbf{f}^{\mathrm{C}}_{ii}(\mathbf{x}_i, \mathbf{x}_i)}{\partial \psi_i} = \frac{\partial \psi_i}{\partial \psi_i} = 1 \tag{3.28}$$

$$\frac{\partial \mathbf{f}^{\mathrm{R}}_{ij}(\mathbf{x}_i, \mathbf{x}_j)}{\partial \mathbf{p}_i} = \frac{\partial \mathbf{R}(\psi_i)(\mathbf{p}_j - \mathbf{p}_i)}{\partial \mathbf{p}_i} = -\mathbf{R}(\psi_i) \tag{3.29}$$

$$\frac{\partial \mathbf{f}^{\mathrm{R}}_{ij}(\mathbf{x}_i, \mathbf{x}_j)}{\partial \mathbf{p}_j} = \frac{\partial \mathbf{R}(\psi_i)(\mathbf{p}_j - \mathbf{p}_i)}{\partial \mathbf{p}_j} = \mathbf{R}(\psi_i) \tag{3.30}$$

$$\frac{\partial \mathbf{f}^{\mathrm{R}}_{ij}(\mathbf{x}_i, \mathbf{x}_j)}{\partial \psi_i} = \frac{\partial \mathbf{R}(\psi_i)(\mathbf{p}_j - \mathbf{p}_i)}{\partial \psi_i} = \boldsymbol{\mu}_{ij} \tag{3.31}$$

where we for ease of notation have introduced $\boldsymbol{\mu}_{ij} = \mathbf{R}(\psi_i + \pi/2)(\mathbf{p}_j - \mathbf{p}_i)$, and where $\mathbf{I}_2$ represent the 2×2 identity matrix. Based on this, we can then express the Jacobian matrix $\nabla_{\boldsymbol{\theta}} \mathbf{f}(\boldsymbol{\theta})$ as

$$\nabla_{\boldsymbol{\theta}} \mathbf{f}(\boldsymbol{\theta}) = \begin{bmatrix} \mathbf{I}_2 & \mathbf{0}_{2,2} & \mathbf{0}_{2,2} & \mathbf{0}_{2,1} & \mathbf{0}_{2,1} & \mathbf{0}_{2,1} \\ \mathbf{0}_{1,2} & \mathbf{0}_{1,2} & \mathbf{0}_{1,2} & 1 & 0 & 0 \\ -\mathbf{R}(\psi_1) & \mathbf{R}(\psi_1) & \mathbf{0}_{2,2} & \boldsymbol{\mu}_{12} & \mathbf{0}_{2,1} & \mathbf{0}_{2,1} \\ -\mathbf{R}(\psi_1) & \mathbf{0}_{2,2} & \mathbf{R}(\psi_1) & \boldsymbol{\mu}_{13} & \mathbf{0}_{2,1} & \mathbf{0}_{2,1} \\ \mathbf{0}_{2,2} & \mathbf{I}_2 & \mathbf{0}_{2,2} & \mathbf{0}_{2,1} & \mathbf{0}_{2,1} & \mathbf{0}_{2,1} \end{bmatrix} \tag{3.32}$$

where $\mathbf{0}_{m,n}$ represent the $m \times n$ zero matrix. Inserting the obtained matrices in (3.26) and performing the matrix multiplications results in a FIM on the form

$$\mathbf{J}(\boldsymbol{\theta}) = \begin{bmatrix} \boldsymbol{\Sigma}_{11}^{-1} + \mathbf{S}_{12} + \mathbf{S}_{13} & -\mathbf{S}_{12} & -\mathbf{S}_{13} & -\mathbf{T}_{12} - \mathbf{T}_{13} & \mathbf{0}_{2,1} & \mathbf{0}_{2,1} \\ -\mathbf{S}_{12} & \boldsymbol{\Sigma}_{22}^{-1} + \mathbf{S}_{12} & \mathbf{0}_{2,2} & \mathbf{T}_{12} & \mathbf{0}_{2,1} & \mathbf{0}_{2,1} \\ -\mathbf{S}_{13} & \mathbf{0}_{2,2} & \mathbf{S}_{13} & \mathbf{T}_{13} & \mathbf{0}_{2,1} & \mathbf{0}_{2,1} \\ -\mathbf{T}_{12}^{\mathrm{T}} - \mathbf{T}_{13}^{\mathrm{T}} & \mathbf{T}_{12}^{\mathrm{T}} & \mathbf{T}_{13}^{\mathrm{T}} & \frac{1}{\sigma_{C,1}^2} + \mathbf{V}_{12} + \mathbf{V}_{13} & 0 & 0 \\ \mathbf{0}_{1,2} & \mathbf{0}_{1,2} & \mathbf{0}_{1,2} & 0 & 0 & 0 \\ \mathbf{0}_{1,2} & \mathbf{0}_{1,2} & \mathbf{0}_{1,2} & 0 & 0 & 0 \end{bmatrix} \tag{3.33}$$

in which $\mathbf{S}_{ij} = \mathbf{R}^{\mathrm{T}}(\psi_i)\boldsymbol{\Sigma}_{ij}^{-1}\mathbf{R}(\psi_i)$, $\mathbf{T}_{ij} = \mathbf{R}^{\mathrm{T}}(\psi_i)\boldsymbol{\Sigma}_{ij}^{-1}\boldsymbol{\mu}_{ij}$, and $\mathbf{V}_{ij} = \boldsymbol{\mu}_{ij}^{\mathrm{T}}\boldsymbol{\Sigma}_{ij}^{-1}\boldsymbol{\mu}_{ij}^{\mathrm{T}}$.

The diagonal blocks in this matrix, can be interpreted as the information that the observations carry about the respective parameters, given that the other parameters are known, while the off diagonal blocks relate to the reduction of information due to uncertainties in the other parameters. For instance, the first diagonal block in $\mathbf{J}(\boldsymbol{\theta})$, correspond to the information that the observations carry about $\mathbf{p}_1$ given that the other parameters are known, while the last diagonal block correspond to the information that the observations carry about ψ_3 given that all the other parameters are known. With this in mind, and to provide some intuition about the different elements in the FIM, we now, as an example, take a closer look at the first diagonal entry in $\mathbf{J}(\boldsymbol{\theta})$. As can be seen it consists of three terms, i.e.,

$$[\mathbf{J}(\boldsymbol{\theta})]_{1,1} = \underbrace{\boldsymbol{\Sigma}_{11}^{-1}}_{\substack{\text{GNSS} \\ \text{observation}}} + \underbrace{\mathbf{S}_{12}}_{\substack{\text{radar} \\ \text{observation} \\ \text{of veh 2}}} + \underbrace{\mathbf{S}_{13}}_{\substack{\text{radar} \\ \text{observation} \\ \text{of veh 3}}} \tag{3.34}$$

The first term, correspond to the information from vehicle one's own GNSS observation, which directly amounts to the inverse of the GNSS observation covariance. The second and third term correspond to the information from the radar observations of vehicle two and three, where $\mathbf{S}_{ij}$, can be interpreted as the radar observation covariance $\boldsymbol{\Sigma}_{ij}$ represented in the global coordinate frame.

Identifiability

The measurements might not carry sufficient information to identify all the unknown parameters in $\boldsymbol{\theta}$. In this specific case, we observe that the last two rows and columns in the FIM are all zero. This means that the parameters ψ_2 and ψ_3 are unidentifiable, and that the FIM is singular, i.e., it can not be inverted in its current form. In general, this is solved by reducing the FIM, first by removing rows and columns corresponding to the unidentifiable parameters, and secondly by removing all contributions in the FIM that comes from measurements involving unidentifiable parameters. In this case, none of

the measurements are connected to ψ_2 and ψ_3, thus to obtain an invertible FIM, we can simply reduce the parameter space by removing the last two rows and columns. After doing this the FIM can be inverted to obtain CRLBs on the remaining parameters.

EFIM

While the CRLBs on the identifiable parameters can be obtained by directly inverting the FIM, the notion of EFI can in general be used to alleviate computational complexity and to further analyze what information the different observations carry about a specific parameter or subspace of parameters. One could for example compute the EFIM $\mathbf{J}_\mathrm{e}(\mathbf{P})$ for the position subspace $\mathbf{P} = \begin{bmatrix}\mathbf{p}_1^\mathrm{T} & \mathbf{p}_2^\mathrm{T} & \mathbf{p}_3^\mathrm{T}\end{bmatrix}^\mathrm{T}$ to reduce computational complexity. However, due to the small size of the problem, there is not really a need for this here, and it might be more interesting to instead break it down on individual vehicle positions. For instance, we can compute the EFIM for vehicle 1's position as

$$\mathbf{J}_\mathrm{e}(\mathbf{p}_1) = \mathbf{A} - \mathbf{B}\mathbf{C}^{-1}\mathbf{B}^\mathrm{T} \tag{3.35}$$

where

$$\mathbf{A} = \mathbf{\Sigma}_{11}^{-1} + \mathbf{S}_{12} + \mathbf{S}_{13} \tag{3.36}$$

$$\mathbf{B} = \begin{bmatrix}-\mathbf{S}_{12} & -\mathbf{S}_{13} & -\mathbf{T}_{12} - \mathbf{T}_{13}\end{bmatrix} \tag{3.37}$$

$$\mathbf{C} = \begin{bmatrix}\mathbf{\Sigma}_{22}^{-1} + \mathbf{S}_{12} & \mathbf{0}_{2,2} & \mathbf{T}_{12} \\ \mathbf{0}_{2,2} & \mathbf{S}_{13} & \mathbf{T}_{13} \\ \mathbf{T}_{12}^T & \mathbf{T}_{13}^T & \frac{1}{\sigma_{C,1}^2} + \mathbf{V}_{12} + \mathbf{V}_{13}\end{bmatrix}. \tag{3.38}$$

From (3.35), we see that information about $\mathbf{p}_1$ is reduced by $\mathbf{B}\mathbf{C}^{-1}\mathbf{B}^\mathrm{T}$ due to uncertainties in the other parameters. Whether or not the expression in (3.35) is tractable or not mainly depends on the structure of $\mathbf{C}$. The EFIMs $\mathbf{J}_\mathrm{e}(\mathbf{p}_1)$ and $\mathbf{J}_\mathrm{e}(\mathbf{p}_2)$ can be computed in a similar manner by appropriate selection of the matrices $\mathbf{A}$, $\mathbf{B}$ and $\mathbf{C}$.

Numerical Results

In this section, we will look at two different variations of the three vehicle scenario and study how the obtained CRLBs and PEBs depend on how the vehicles are positioned in relation to each other. To do this we fix the parameters of the sensors according to Table 3.2. In the first variation of the scenario, we let $\mathbf{p}_1 = \begin{bmatrix}9 & -2\end{bmatrix}^\mathrm{T}$, $\mathbf{p}_2 = \begin{bmatrix}35 & 6\end{bmatrix}^\mathrm{T}$, $\mathbf{p}_3 = \begin{bmatrix}50 & 2\end{bmatrix}^\mathrm{T}$, $\psi_1 = 0$, $\psi_2 = 180$ and $\psi_3 = 180$. The results for this case are visualized in Figure 3.6, which shows the true locations of the vehicles along with 1-sigma uncertainty ellipses corresponding to the obtained CRLBs. Also indicated in the figure are the respective PEBs. We observe that vehicle 1 and 2 get the same PEB of 2.45 m, while the PEB for vehicle 3 is 3.53 m. In other words, using a cooperative approach it is possible

Table 3.2. Sensor parameters

Parameters	Values
GNSS position unc. (m)	$\sigma_{\mathrm{G}} = 2$
Compass heading unc. (deg)	$\sigma_{\mathrm{C}} = 1$
Radar opening angle (deg)	$\theta_{\mathrm{FOV}} = 45°$
Radar max range (m)	$r_{\max} = 45$
Radar range unc. (m)	$\sigma_r = 0.12$
Radar bearing unc. (deg)	$\sigma_\alpha = 0.3°$

to position vehicle 3 even though it does not contribute with any observations. We also note that if we, for instance, look at the ellipse for vehicle 1, we have less uncertainty along the direction towards vehicle 2. This is because the accurate range measurement of the radar.

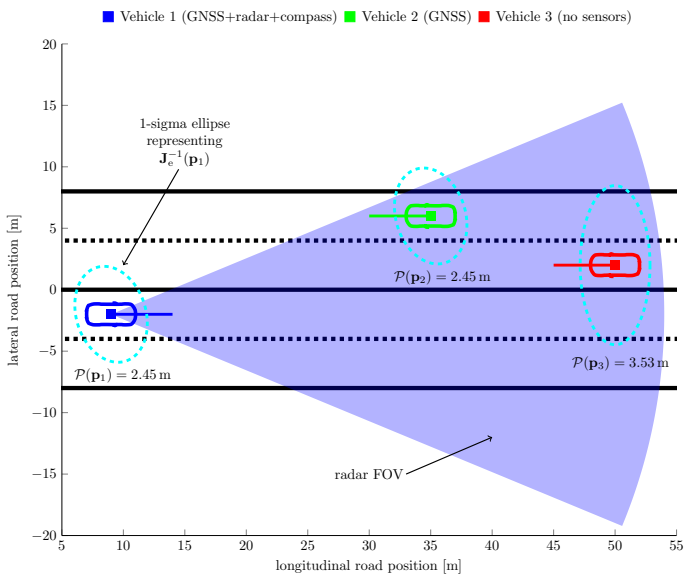

Figure 3.6. Visualization of obtained CRLBs and PEBs for the case when the true positions of the vehicles are $\mathbf{p}_1 = \begin{bmatrix}9 & -2\end{bmatrix}^{\mathrm{T}}$, $\mathbf{p}_2 = \begin{bmatrix}35 & 6\end{bmatrix}^{\mathrm{T}}$, and $\mathbf{p}_3 = \begin{bmatrix}50 & 2\end{bmatrix}^{\mathrm{T}}$. CRLBs are visualized in form of 1-sigma uncertainty ellipses.

To show that the obtain CRLBs and PEBs depend on the true vehicle positions, we now let vehicle 2 and vehicle 3 swap positions, i.e., we set $\mathbf{p}_2 = \begin{bmatrix}50 & 2\end{bmatrix}^{\mathrm{T}}$ and $\mathbf{p}_3 = \begin{bmatrix}35 & 6\end{bmatrix}^{\mathrm{T}}$. Results for this case are visualized in Figure 3.7. Interestingly, and maybe a bit counter intuitively, we see that in this case vehicle 3 has the lowest PEB. In other words, we

can position the vehicle that don't explicitly contribute with any measurements more accurately than the other. This is an effect of how the measurements are correlated.

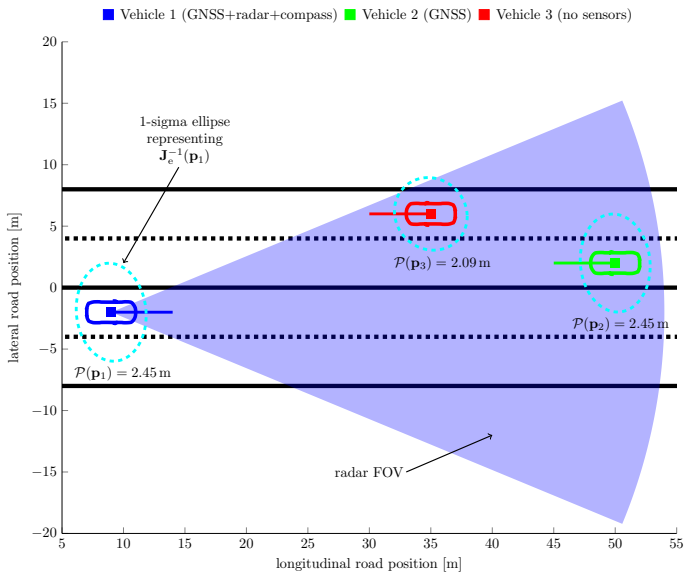

Figure 3.7. Visualization of obtained CRLBs and PEBs for the case when the true positions of the vehicles are $\mathbf{p}_1 = [9 \quad -2]^{\mathrm{T}}$, $\mathbf{p}_2 = [50 \quad 2]^{\mathrm{T}}$, and $\mathbf{p}_3 = [35 \quad 6]^{\mathrm{T}}$. CRLBs are visualized in form of 1-sigma uncertainty ellipses.

3.6 Summary

Positioning in future ITS will most likely rely on (i) a combination of sensor technologies; (ii) cooperative strategies where vehicles share sensor data over the wireless channel. An important question is, however, whether or not this is sufficient to meet the positioning requirements posed by safety critical ITS applications. In this chapter, we have introduced the concept of Fisher Information and Cramér-Rao bounds, and showed how these tools can be used to provide insights about what is theoretically possible.

In paper G, we utilize the tools presented in this chapter to gain fundamental insight about how the sensing capability in a vehicle fleet impacts positioning and mapping performance, and how different types of observations contribute in reducing the positioning uncertainty.

CHAPTER 4

Control

In this chapter, we will provide the reader with a basic understanding of how the control problem can be formalized. We will also review the concept of model predictive control (MPC), and discuss the impact of communication and sensing uncertainties.

4.1 The Control Problem

Considering a set of vehicles, the control problem can simply be seen as the task of computing the best control input trajectories for individual vehicles that allow them to safely reach their destination in a finite time. In other words, we want to find control input trajectories that satisfy basic safety and liveness requirements, and at the same time, minimize some performance criterion, such as energy consumption, driver discomfort or deviation from target speed. As pointed out in Paper E, one way to look at this problem is as a constrained optimal control problem, i.e.,

$$\begin{aligned} \underset{\text{vehicle controls}}{\text{minimize}} \quad & \text{performance criterion} && \text{(4.1a)} \\ \text{subject to} \quad & \text{vehicle dynamics} && \text{(4.1b)} \\ & \text{safety constraints} && \text{(4.1c)} \\ & \text{liveness constraints} && \text{(4.1d)} \end{aligned}$$

where the safety constraints (4.1c) make sure that no collisions occur, and the liveness constraints (4.1d) guarantee that no traffic dead locks happen and vehicles eventually reach their destination.

4.2 Model Predictive Control

Model predictive control (MPC), sometimes also referred to as receding horizon control (RHC), has its roots in optimal control, and is an optimization based control technique where control inputs are computed based on observations of the current system state, and predicted state trajectories. More specifically, a dynamical model of the system is used to predict state trajectories, and solve an open loop optimal control problem, where some form of performance criterion is minimized, over a finite future horizon of N steps. Solving the open loop control problem gives the sequence of control inputs that minimizes the performance criterion over the prediction horizon. In MPC the first control input is then typically applied. The system then moves to a new state, and after observation of the new state, a new open loop control problem is solved over a shifted horizon, to find the control input for the next time step. The basic principle of MPC is illustrated in Figure 4.1. A more in depth description of MPC can be found in, for example, [83].

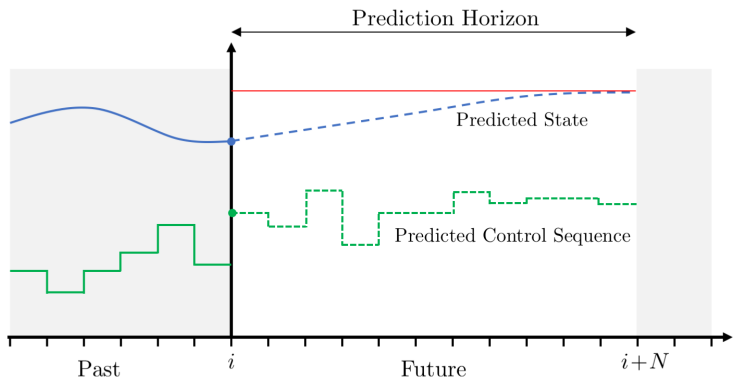

Figure 4.1. Illustration of the basic principle of MPC

4.3 Communication and Sensing Uncertainties

While we in Paper E present results on how communication and sensing uncertainties impacts the task of controlling two vehicles seamlessly through an intersection, we will here consider a simple abstraction of this scenario. Both to see how communication and sensing uncertainties affects the control task, and to give the reader a concrete example of what a simple MPC problem could look like. We will also briefly discuss existing strategies for dealing with communication and sensing uncertainties.

4.3.1 Scenario Description

In this example, we consider the task of controlling a single vehicle such that it crosses an intersection by a given deadline time t_{exit}. The vehicle is assumed to communicate with and be controlled by a central intersection manager (IM). For simplicity, we also assume that the vehicle follows a pre-determined path such that its motion can be considered one dimensional, and that the exit point of the intersection is denoted x_{exit}. An illustration of the scenario is shown in Figure 4.2.

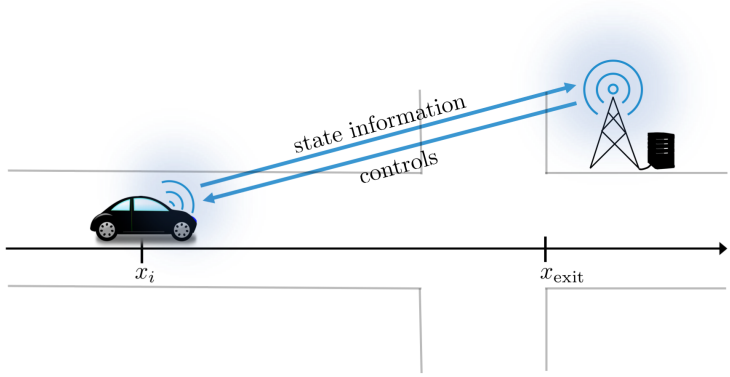

Figure 4.2. Illustration of the scenario

By assuming that time is discretized with sample time T_{s}, and that the vehicle should from where it starts have left the intersection at the end of the prediction horizon (i.e., at time step N) the open loop control problem can be expressed as [84]

$$\begin{aligned}
\underset{\mathbf{u}_i}{\text{minimize}} \quad & \sum_{k=0}^{N-1} u_{i,k}^2 && \text{(4.2a)}\\
\text{subject to} \quad & \mathbf{x}_{i,0} = \hat{\mathbf{x}}_i && \text{(4.2b)}\\
& \mathbf{x}_{i,k+1} = \mathbf{A}_i \mathbf{x}_{i,k} + \mathbf{b}_i u_{i,k} && \text{(4.2c)}\\
& x_{i,N-i} \geq x_{\text{exit}} + \varepsilon && \text{(4.2d)}
\end{aligned}$$

in which $\mathbf{x}_{i,k} = [x_{i,k} \; v_{i,k}]^{\text{T}}$ represent the state of the vehicle, comprising the scalar position $x_{i,k}$ and velocity $v_{i.k}$, where the time index i refers to the current time and the time index k refers to the time along the prediction horizon. In other words, the control signal computed at time i is $\mathbf{u}_i = [u_{i,0}, \ldots, u_{i,N-1}]$. The constraint (4.2c) describes the motion dynamics of the vehicle, and the constraint (4.2d) aims to make sure that the vehicle leaves the intersection before the deadline, to avoid potential collisions with the vehicles arriving at the intersection after time t_{exit}. Note that as we assume that the true vehicle dynamics are subject to a stochastic perturbation $\mathbf{w}_i \sim \mathcal{N}(0, \mathbf{Q})$, we have added

a safety margin ε to obtain a safe behavior in the situation without communication and sensing uncertainties. The selected performance criteria (4.2a) is in this case to minimize the squared norm of the control signal, which in principle can be seen as a simple way of minimizing the consumed energy and maximizing the passenger comfort. Furthermore, the constraint (4.2b) defines the starting point, i.e., the initial state, from which the problem is solved.

To study the impact of sensing communication uncertainties we assume that the vehicle at each time instance i makes noisy observations

$$\mathbf{y}_i = \mathbf{x}_i + \mathbf{n}_i \tag{4.3}$$

of its state, where $\mathbf{n}_i \sim \mathcal{N}(0, \mathbf{R})$, and send these to the IM on an uplink channel. The IM runs a tracking filter, and as soon as it receives a packet from the vehicle computes an estimate $\hat{\mathbf{x}}_i$ of the vehicles state based on all the observations received up until time i. Using this as a starting point for the problem in (4.2), it then computes a control sequence $\mathbf{u}_i = [u_{i,0}, \ldots, u_{i,N-1}]$ and sends this back to the vehicle on a downlink (DL) channel. Both UL and DL communication is assumed to be unreliable with a packet loss probability of $p \in [0, 1]$. Furthermore, we assume that the vehicle applies the computed control sequence as long as no new control sequence is received. In other words, when a DL packet is lost, the vehicle follows the old control sequence. However, when a UL packet is lost, the IM computes and broadcasts a new control sequence based on a state prediction from the tracking filter. Furthermore, we assume that the vehicle does not apply any control command until tracking is initialized and it receives its first control sequence. Finally, we also define all time instances that the vehicle does not cross the intersection in time as collisions.

As a remark, it can be mentioned that the problem of coordinating vehicles in an intersection in general can be decomposed into a high-level problem of assigning time slots and a low-level control problem of making sure that the vehicles cross the intersection during the assigned time slots [85]. The simple problem studied here can be seen as an abstraction of the low-level control part.

4.3.2 Numerical Results

To show the effect of communication and sensing uncertainties we now present results from Monte Carlo simulations where we study the collision probability, i.e., the probability that the vehicle does not cross the intersection in time, and the average control cost. In these simulations, we assume a sample time $T_\mathrm{s} = 0.5$ s and that the vehicle at time instance $i = 0$ starts 100 m away from the intersection with a speed of 1 m/s, and $N = 20$ time step later should have crossed the intersection. We let $\varepsilon = 0.5$ m. Furthermore, we consider the same process noise as in [84] and assume that we in this

case only have noise on the observation of the vehicles position, such that

$$\mathbf{Q} = \begin{bmatrix} 0.0104 & 0.0313 \\ 0.0313 & 0.1250 \end{bmatrix}, \ \mathbf{R} = \begin{bmatrix} \sigma_p^2 & 0 \\ 0 & 0 \end{bmatrix}, \tag{4.4}$$

where σ_p correspond to the standard deviation of the position noise. For visualization purposes, we also consider the control cost to be the sum of the applied control actions, even though (4.2) minimizes the sum of the squared control actions.

Figure 4.3 shows how the collision probability and the average control cost depends on the packet loss probability p and the uncertainty in the observation of the vehicles position σ_p. As can be seen, the collision probability increases with both increased position uncertainty σ_p and packet loss probability p. We also note that losing all packets, i.e., $p = 1$, results in a collision probability of one as the vehicle due to its low initial velocity never crosses the intersection on time. Regarding the average control cost, we see a slight increase due to increased position uncertainty. However, when it comes to the effect of packet losses, we see a significant increase in the average control cost as the packet loss probability increases. This is due to the fact that errors are accumulated over time as consecutive packets are lost, and that a large control action needs to be applied in order to compensate for this. In other words, it shows the effect of reduced feedback. We also note that when all packets are lost, the average control cost is zero, as no control action is applied then.

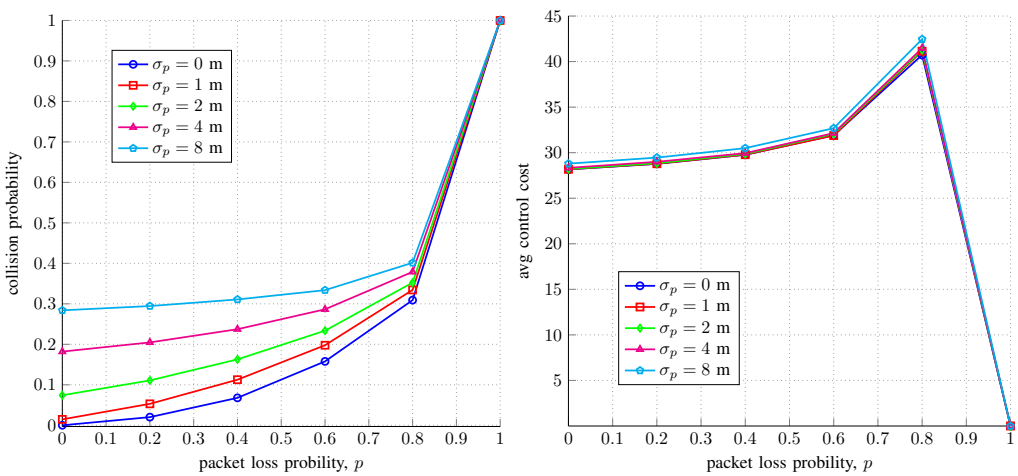

(a) **(b)**

Figure 4.3. Control performance in terms of (a) collision probability and (b) control cost as a function of packet loss probability p for different positioning uncertainties $\sigma_p \in \{0\,\text{m}, 1\,\text{m}, 2\,\text{m}, 4\,\text{m}, 8\,\text{m}\}$. Results are based on simulations with 10000 realizations for each parameter combination.

4.3.3 Solution Strategies

As we saw in Section 4.3.2, two important aspects when it comes to the performance of a control system is the safety of the system, which relates to constraint satisfaction, and the efficiency, i.e., the cost in term of the chosen performance metric. A third important metric is stability, which simply put is the ability of the controller to stabilize the system, so that a bounded deviation between the actual and desired system state can be ensured [83], [86].

With this in mind, let us now consider the case when there are neither sensing nor communication uncertainties, and no modeling uncertainties or external disturbances. In such a case, there is generally no need for feedback [83], i.e., it is sufficient to communicate once as the evolution of the system state can be predicted from the initial state.[1] If we introduce sensing uncertainties (or modeling uncertainties) the controller belief of the system state will, however, deviate from the true system state, and over time be more inexact. It is therefore desirable to minimize the impact of these uncertainties with feedback. With communication uncertainties feedback might however be intermittent. One part in the puzzle is thus to look at how little feedback that can be tolerated, such as in [17], [18]. These works mainly addresses stability, but can in principle be used to put formal requirements on the underlying communication system, and design resource allocation schemes that makes sure that necessary communication resources are allocated. Connected to this is for example [19], where communication resources are allocated to minimize the expected increase in instability of a constrained control system. Good to have in mind though, is that while stability is important, it may not be sufficient to guarantee safety, neither does it maximize the efficiency of the system. Thus, a more interesting problem is how much feedback that is necessary to guarantee safety and minimize the performance cost. Part of this problem is addressed in [20]–[22], which through the use of the two related concepts value of information (VoI) and cost of information loss (CoIL), considers the cost in terms of the chosen performance metric.

Another, approach to deal with both communication and sensing uncertainties is to use robust control formulations, which explicitly accounts for state uncertainties. In this category, falls works such as [12]–[15], that rely on reachability analysis for propagation of uncertainties to compute unsafe regions (so-called capture sets) in the state space that should be avoided. Another example is robust MPC (e.g. [16], [87]), which guarantees constraint satisfaction given bounded state uncertainties, and thus reduces the need for feedback. Drawbacks with robust MPC, compared to nominal MPC, is its relatively high computational complexity, and that it tends to be more conservative. The main reasons for this conservativeness is that uncertainties have to be propagated along the prediction horizon, and that persistent feasibility [88] must be guaranteed in a robust way, i.e., it should for upcoming time instances be possible to find a solution that satisfies the system constraints. The conservativeness can however to some extent be mitigated by relying

[1] Note that if finite horizon approximations are used, or if the controller need to be able to handle that additional vehicles appear it might still be desirable with some feedback

on stochastic MPC approaches [84], [89], where constraint violations are tolerated with some small probability.

4.4 Summary

In this chapter, we have seen that the task of coordinating vehicles can be cast as an constrained optimal control problem, and how communication and sensing uncertainties can impact control performance. Furthermore, we have learned that when it comes to accounting for communication and sensing uncertainties the coin is two sided. In one way, it is for a given control application possible to put requirements on the underlaying communication and sensing systems. On the other hand, through a better understanding of what the limitations are in regards to communication and sensing in different situations, it is also possible to design controllers that explicitly account for the associated uncertainties. Finally, we have also learned that in addition to stability it is important to consider safety, i.e., constraint satisfaction, as well as the efficiency in terms of the defined performance metric.

In Paper E, we provide study of how communication and sensing uncertainties impacts the task cooperative intersection coordination. In Paper B and E, we aim to reduce the gap between the communication, sensing and control systems. In Paper B, we use stochastic geometry to analyze how controller, and quality of service requirements, influences communication system design. In Paper E, we propose a resource allocation strategy that proactively assigning communication resources based on risks for future collisions, i.e., we explicitly consider safety requirements.

CHAPTER 5

Scientific Achievements, Conclusions and Outlook

This thesis studies communication and sensing uncertainties in the context of cooperative ITS. The contributions of this thesis include:

- analytical models for the reliability of packet transmissions in vehicular networks, based on a stochastic geometry interference analysis;
- bounds on the achievable performance of cooperative positioning solutions in future ITS, based on a Fisher information theory approach;
- a study on how communication and sensing impacts safety, and a communication resource allocation method that explicitly accounts for safety.

In Part II, the author's contributions of the thesis in terms of publications are presented. In the following, we provide a summary of the scientific achievements, conclusions and discuss possible extensions of this thesis' work.

5.1 Analytical Models on Packet Reception Probabilities (Paper A, C and D)

To be able to guide and validate the design of vehicular communication system and to gain fundamental insights about what the performance is in different situations, analytical expressions of key performance metrics such as packet reception probabilities and throughput are necessary. Especially, for high velocity scenarios (e.g., highways), and accident prone scenarios (e.g., intersections). In Papers A, C and D, we use tools

from stochastic geometry to capture the spatial statistics of the vehicles and analyze the impact of interference in vehicular networks.

In Paper A, which is a work in progress abstract, we consider a four lane intersection scenario where each lane carries cars according to a one dimensional homogeneous PPP. Given this scenario, and the assumption of exponential power fading and an Aloha MAC protocol, we present an analytical model for the reliability of packet transmissions on a selected link. In Paper C, we show how the model, due to the independence of the PPPs on the different lanes, can be extended to account for an arbitrary number of lanes with different orientations. We also explore the possibility to account for increased vehicle densities near the intersection, caused by for example reduced vehicle speeds and traffic congestions, and show how closed form expressions still can be obtained for special cases such as piecewise linear densities, even when the PPP is non-homogeneous. Finally in Paper D, we extend and give a more complete presentation of the work in Paper A and C. In particular, we present a general procedure to analytically evaluate the packet reception probability and throughput of a selected link, and provide a model repository that can be used to adapt to both urban and rural propagation characteristics (with LOS blockage and shadowing), as well as different MAC protocols (Aloha and CSMA/CA).

We have applied and validated this procedure to three case studies, relevant for vehicular applications, and we find that the clear structure of the scenario, with two roads that cross, leads to location-dependent packet reception probabilities and throughputs. We also find that the procedure is sufficiently general and flexible and can capture the performance of realistic scenarios well, provided the modeling assumptions hold true.

The proposed models are mainly applicable to 802.11p communication, thus possible avenues for future research includes adoption of advanced MAC schemes as well as 5G D2D features, and validation of the model against actual measurements.

5.2 Bounds on Cooperative Positioning in ITS (Paper G)

Accurate positioning and real-time situational awareness are key in future ITS, and along with higher levels of automation comes an increased demand on an accurate representation of the surrounding environment. An important question is how we meet these demands, and what performance we can expect from positioning systems in future ITS?

Cooperative positioning solutions, where vehicles share sensor information over the wireless channel, are foreseen to play an important role in meeting these demands. In Paper G, we provide a framework and method based on Fisher information analysis and Cramér-Rao bounds to determine the fundamental limits for cooperative positioning in a scenario, where vehicles share information from on-board GNSS, compass, and radar sensors. In particular we study the effect of a gradual market penetration, and show how the composition of the vehicle fleet, and the penetration rate of vehicles with extensive sensing capability, affects the positioning performance. While the analysis is generally applicable, we present simulation results from a multi-lane freeway scenario. These results

indicate that solely introducing a small fraction of automated vehicles with high-end sensors significantly improves the positioning quality, but is not enough to meet the stringent demands posed by safety critical ITS applications. Other insights that we can obtain from the simulations are that simple measures such as retrofitting vehicles with low-cost GNSS and communication have marginal impact when the positioning requirements are stringent, and that longitudinal road position can be estimated more accurately than lateral given the assumed sensor configuration.

Possible avenues for future research extensions include (i) incorporation of realistic model for sensor blockage; (ii) extension to dynamic scenarios with tracking; (iii) incorporation of advanced sensor models and extended objects.

5.3 Impact of Uncertainties and Control and Sensing Aware Communication (Paper B, E and F)

In Paper E, we present a study of how sensing and communication uncertainties impacts the task of cooperative intersection coordination. From this study, and the discussion in the paper, we see that if the control communication and sensing systems are treated separately, the requirements on each of the subsystems are stringent in order to be able to guarantee safety. By making the subsystems aware of each other it might, however, to some extent be possible to relax these constraints. In Paper B and F, we explore this.

In Paper B, we provide a communication system analysis for a centralized intersection coordination scheme, using tools from stochastic geometry. Specifically, we characterize the probability that the controller receives state information sent from the vehicles (on an uplink channel) within a certain region around the controller. Similarly, we characterize the downlink probability, i.e., the probability that the vehicles receives information within a certain region around the controller. Using this we then provide guidelines on how to design the communication system, to fulfill certain quality of service (QoS) requirements posed by the controller. Note that QoS in this context relates to the probability that the controller and the vehicles receive the information within the assigned regions. In other words, we show how awareness about controller requirement impacts communication system design. Conversely the tools developed can also be used to study how far away from the intersection the controller can expect to have information available from all vehicles given certain communication parameters, QoS requirements, vehicle densities and velocities.

While the specifications of the controller are kept general in Paper B, Paper F considers intersection coordination with a predictive controller, such as MPC. In particular, we propose a collision aware resource allocation strategy (CARA). This strategy relies on a new concept referred to as collision possibility indicator (CPI), which characterizes risk of collisions for pairs of vehicles. The CPI accounts for state uncertainty as well as the dynamics of the vehicles, and by evaluating the CPIs over the prediction horizon,

we establish when its necessary to communicate in order to rule out the possibility of future collisions. By using the CPIs, the proposed strategy proactively reduces the risk of channel congestion, by only assigning communication resources to vehicles that are in critical configurations, i.e., when there is a risk for a future collision. Specifically, we find that compared to traditional collision-agnostic communication schemes with fixed transmission intervals, the proposed CARA strategy significantly reduces the amount of communication (albeit with a slight increase in control cost), without compromising safety. We also present a trade-off analysis where we show how control cost can be reduced at the cost of increased communication load.

Possible avenues for future research include: (i) incorporation of bandwidth constraints such that only a limited number of agents can transmit in each time slot; (ii) making the collision-aware resource allocation strategy robust to communication imperfections such as packet drops and delays; (iii) investigate the feasibility for scenarios with multiple vehicles on the same path; (iv) explicitly accounting for control performance in addition to collision possibilities.

5.4 Author Contributions of Appended Papers

5.4.1 Paper A

M. Wildemeersch (MW) proposed the problem. E. Steinmetz (ES) derived the model with support from MW and H. Wymeersch (HW).

5.4.2 Paper B

ES derived the analytical expressions and performed the analysis together with MW and HW. R. Hult (RH), G. Rodrigues de Campos (GRDC) and P. Falcone (PF) participated in the discussion and collaborated with paper writing.

5.4.3 Paper C

ES derived the analytical expressions and performed the simulations with support from MW and HW. T. Q. S. Quek (TQSQ) participated in the discussion and collaborated with paper writing.

5.4.4 Paper D

ES derived the analytical expressions and performed the simulations. MW, TQSQ and HW participated in the discussion and collaborated with paper writing.

5.4.5 Paper E

ES performed the study on how communication sensing uncertainties affects control performance, and with support from HW wrote the sections relating to communication.

5.4.6 Paper F

ES proposed and implemented the resource allocation algorithm, and performed the simulations. RH supported with the implementation of the controller. Z. Zou (ZZ) assisted with the analytical characterization of the capture set. R. Emardson (RE), F. Brännström (FB), PF and HW participated in the discussion and collaborated with paper writing.

5.4.7 Paper G

ES performed the analysis and implemented the simulations. RE, FB an HW participated in the discussion and collaborated with paper writing.

References

[1] World Health Organization (WHO), "Global Status Report on Road Safety", 2018.

[2] D. Schrank and B. Eisele and T. Lomax and J. Bak, "2015 Urban Mobility Scorecard", Texas A&M Transportation Institute and INRIX, 2015.

[3] Intergovernmental Panel on Climate Change (IPCC), "Climate Change 2014: Mitigation of Climate Change", 2014.

[4] M. Gerla, E. Lee, G. Pau, and U. Lee, "Internet of vehicles: From intelligent grid to autonomous cars and vehicular clouds", in *2014 IEEE World Forum on Internet of Things (WF-IoT)*, 2014, pp. 241–246.

[5] H. Hartenstein and K. P. Laberteaux, "A tutorial survey on vehicular ad hoc networks", *IEEE Communications Magazine*, vol. 46, no. 6, pp. 164–171, 2008.

[6] L. Kong, M. K. Khan, F. Wu, G. Chen, and P. Zeng, "Millimeter-Wave Wireless Communications for IoT-Cloud Supported Autonomous Vehicles: Overview, Design, and Challenges", *IEEE Communications Magazine*, vol. 55, no. 1, pp. 62–68, 2017.

[7] K. Sjoberg, P. Andres, T. Buburuzan, and A. Brakemeier, "Cooperative Intelligent Transport Systems in Europe: Current Deployment Status and Outlook", *IEEE Vehicular Technology Magazine*, vol. 12, no. 2, pp. 89–97, 2017.

[8] L. Chen and C. Englund, "Cooperative intersection management: A survey", *IEEE Transactions on Intelligent Transportation Systems*, vol. 17, no. 2, pp. 570–586, 2016.

[9] G. R. de Campos, P. Falcone, R. Hult, H. Wymeersch, and J. Sjöberg, "Traffic coordination at road intersections: Autonomous decision-making algorithms using model-based heuristics", *IEEE Intelligent Transportation Systems Magazine*, vol. 9, no. 1, pp. 8–21, 2017.

[10] S. Kim, W. Liu, M. H. Ang, E. Frazzoli, and D. Rus, "The Impact of Cooperative Perception on Decision Making and Planning of Autonomous Vehicles", *IEEE Intelligent Transportation Systems Magazine*, vol. 7, no. 3, pp. 39–50, 2015.

[11] M. Rockl, T. Strang, and M. Kranz, "V2V Communications in Automotive Multi-Sensor Multi-Target Tracking", in *IEEE 68th Vehicular Technology Conference*, 2008, pp. 1–5.

[12] D. Bresch-Pietri and D. D. Vecchio, "Estimation for decentralized safety control under communication delay and measurement uncertainty", *Automatica*, vol. 62, pp. 292–303, 2015.

[13] G. Campos, P. Falcone, H. Wymeersch, R. Hult, and J. Sjöberg, "Cooperative receding horizon conflict resolution at traffic intersections", in *Proceedings of the IEEE 53rd Annual Conference on Decision and Control (CDC)*, 2014.

[14] M. R. Hafner, D. Cunningham, L. Caminiti, and D. Del Vecchio, "Cooperative collision avoidance at intersections: Algorithms and experiments", *IEEE Transaction on Intelligent Transportation Systems*, vol. 14, no. 3, pp. 1162–1175, 2013.

[15] M. R. Hafner and D. D. Vecchio, "Computational tools for the safety control of a class of piecewise continuous systems with imperfect information on a partial order", *SIAM Journal on Control and Optimization*, vol. 49, no. 6, pp. 2463–2493, 2011.

[16] R. Arthur George, "Robust Constrained Model Predictive Control", PhD thesis, Massachusetts Institute of Technology, 2005.

[17] L. Schenato, B. Sinopoli, M. Franceschetti, K. Poolla, and S. S. Sastry, "Foundations of control and estimation over lossy networks", *Proceedings of the IEEE*, vol. 95, no. 1, pp. 163–187, 2007.

[18] D. Tolić and S. Hirche, "Stabilizing transmission intervals for nonlinear delayed networked control systems", *IEEE Transactions on Automatic Control*, vol. 62, no. 1, pp. 488–494, 2017.

[19] M. Zanon, T. Charalambous, H. Wymeersch, and P. Falcone, "Optimal scheduling of downlink communication for a multi-agent system with a central observation post", *IEEE Control Systems Letters*, vol. 2, no. 1, pp. 37–42, 2018.

[20] A. Molin, C. Ramesh, H. Esen, and K. H. Johansson, "Innovations-based priority assignment for control over can-like networks", in *54th IEEE Conference on Decision and Control (CDC)*, 2015, pp. 4163–4169.

[21] T. Soleymani, S. Hirche, and J. S. Baras, "Optimal self-driven sampling for estimation based on value of information", in *Proceedings of the 13th International Workshop on Discrete Event Systems (WODES)*, 2016, pp. 183–188.

[22] T. Charalambous, A. Ozcelikkale, M. Zanon, P. Falcone, and H. Wymeersch, "On the resource allocation problem in wireless networked control system", in *IEEE Conference on Decision and Control (CDC)*, 2017.

[23] H. Wymeersch, G. de Campos, P. Falcone, L. Svensson, and E. Ström, "Challenges for cooperative ITS: Improving road safety through the integration of wireless communications, control, and positioning", in *International Conference on Computing, Networking and Communications (ICNC)*, 2015, pp. 573–578.

[24] A. Moller, J. Nuckelt, D. M. Rose, and T. Kurner, "Physical layer performance comparison of lte and ieee 802.11p for vehicular communication in an urban nlos scenario", in *2014 IEEE 80th Vehicular Technology Conference (VTC2014-Fall)*, 2014, pp. 1–5.

[25] H. Tchouankem, T. Zinchenko, and H. Schumacher, "Impact of buildings on vehicle-to-vehicle communication at urban intersections", in *2015 12th Annual IEEE Consumer Communications and Networking Conference (CCNC)*, 2015, pp. 206–212.

[26] C. Sommer, S. Joerer, M. Segata, O. K. Tonguz, R. L. Cigno, and F. Dressler, "How shadowing hurts vehicular communications and how dynamic beaconing can help", *IEEE Transactions on Mobile Computing*, vol. 14, no. 7, pp. 1411–1421, 2015.

[27] C. F. Mecklenbrauker, A. F. Molisch, J. Karedal, F. Tufvesson, A. Paier, L. Bernado, T. Zemen, O. Klemp, and N. Czink, "Vehicular Channel Characterization and Its Implications for Wireless System Design and Performance", *Proceedings of the IEEE*, vol. 99, no. 7, pp. 1189–1212, 2011.

[28] M. Rockl, "Cooperative Situation Awareness in Transportation", PhD thesis, University of Innsbruck, 2009.

[29] F. d. P. Müller, E. M. Diaz, and I. Rashdan, "Cooperative positioning and radar sensor fusion for relative localization of vehicles", in *IEEE Intelligent Vehicles Symposium (IV)*, 2016, pp. 1060–1065.

[30] S. Kim, B. Qin, Z. J. Chong, X. Shen, W. Liu, M. H. Ang, E. Frazzoli, and D. Rus, "Multivehicle Cooperative Driving Using Cooperative Perception: Design and Experimental Validation", *IEEE Transactions on Intelligent Transportation Systems*, vol. 16, no. 2, pp. 663–680, 2015.

[31] Y. Shen, H. Wymeersch, and M. Z. Win, "Fundamental Limits of Wideband Localization; Part II: Cooperative Networks", *IEEE Transactions on Information Theory*, vol. 56, no. 10, pp. 4981–5000, 2010.

[32] H. Wymeersch, G. Seco-Granados, G. Destino, D. Dardari, and F. Tufvesson, "5G mmWave Positioning for Vehicular Networks", *IEEE Wireless Communications*, vol. 24, no. 6, pp. 80–86, 2017.

[33] J. Gabela, S. Goel, A. Kealy, and M. Hedley, "Cramér Rao Bound Analysis for Cooperative Positioning in Intelligent Transportation Systems", in *IGNSS Symposium 2018*, 2018.

[34] H. Li and F. Nashashibi, "Cooperative multi-vehicle localization using split covariance intersection filter", *IEEE Intelligent Transportation Systems Magazine*, vol. 5, no. 2, pp. 33–44, 2013.

[35] R. M. Buehrer, H. Wymeersch, and R. M. Vaghefi, "Collaborative Sensor Network Localization: Algorithms and Practical Issues", *Proceedings of the IEEE*, vol. 106, no. 6, pp. 1089–1114, 2018.

[36] Y. Wang, G. de Veciana, T. Shimizu, and H. Lu, "Performance and Scaling of Collaborative Sensing and Networking for Automated Driving Applications", in *IEEE International Conference on Communications Workshops (ICC Workshops)*, vol. 16, 2018.

[37] S. Oyama, "Activities on ITS Radiocommunications Standards in ITU-R and in Japan", 2009. [Online]. Available: `http://docbox.etsi.org//workshop/2009/200902_itsworkshop/itu_r_oyama.pdf`.

[38] New Zealand Radio Spectrum Management, "Intelligent transport systems in the 5.9 GHz band", 2015. [Online]. Available: `http://www.rsm.govt.nz/projects-auctions/completed/intelligent-transport-systems-in-the-5.9-ghz-band`.

[39] IEEE Std 802.11-2007, "Wireless LAN MAC and PHY Specifications", 2007.

[40] IEEE Std 802.11p-2010, "Amendment 6: Wireless Access in Vehicular Environments", 2010.

[41] IEEE Std 1609.3-2010, "IEEE Standard for Wireless Access in Vehicular Environments-Networking Services", 2010.

[42] ETSI ES 202 663 V1.1.0, "Intelligent Transport Systems (ITS); European profile standard for the physical and medium access control layer of Intelligent Transport Systems operating in the 5 GHz frequency band", 2009.

[43] A. M. S. Abdelgader and W. Lenan, "The Physical Layer of the IEEE 802 . 11p WAVE Communication Standard : The Specifications and Challenges", in *World Congress on Engineering and Computer Science 2014*, vol. II, 2014, pp. 22–24.

[44] J. B. Kenney, G. Bansal, and C. E. Rohrs, "LIMERIC: a linear message rate control algorithm for vehicular DSRC systems", in *Proceedings of the Eighth ACM international workshop on Vehicular inter-networking*, 2011, pp. 21–30.

[45] K. Sjöberg, "Medium Access Control for Vehicular Ad Hoc Networks", PhD thesis, Chalmers University of Technology, 2013.

[46] D. Jiang and L. Delgrossi, "IEEE 802.11p: Towards an International Standard for Wireless Access in Vehicular Environments", in *VTC Spring 2008 - IEEE Vehicular Technology Conference*, 2008, pp. 2036–2040.

[47] J. F. Monserrat, H. Droste, O. Bulakci, J. Eichinger, O. Queseth, M. Stamatelatos, H. Tullberg, V. Venkatkumar, G. Zimmermann, U. Dotsch, and A. Osseiran, "Rethinking the mobile and wireless network architecture: The METIS research into 5G", in *European Conference on Networks and Communications (EuCNC)*, 2014.

[48] S. Mumtaz, K. M. Saidul Huq, and J. Rodriguez, "Direct mobile-to-mobile communication: Paradigm for 5G", *IEEE Wireless Communications*, vol. 21, no. 5, pp. 14–23, 2014.

[49] A. Khelil and D. Soldani, "On the suitability of Device-to-Device communications for road traffic safety", in *IEEE World Forum on Internet of Things (WF-IoT)*, 2014, pp. 224–229.

[50] X. Cheng, L. Yang, and X. Shen, "D2D for Intelligent Transportation Systems: A Feasibility Study", *IEEE Transactions on Intelligent Transportation Systems*, vol. PP, no. 99, pp. 1–10, 2015.

[51] L. Cheng, B. Henty, D. Stancil, F. Bai, and P. Mudalige, "Mobile Vehicle-to-Vehicle Narrow-Band Channel Measurement and Characterization of the 5.9 GHz Dedicated Short Range Communication (DSRC) Frequency Band", *IEEE Journal on Selected Areas in Communications*, vol. 25, no. 8, pp. 1501–1516, 2007.

[52] J. Karedal, N. Czink, A. Paier, F. Tufvesson, and A. F. Molisch, "Path Loss Modeling for Vehicle-to-Vehicle Communications", *IEEE Transactions on Vehicular Technology*, vol. 60, no. 1, pp. 323–328, 2011.

[53] T. Abbas, K. Sjöberg, J. Karedal, and F. Tufvesson, "A measurement based shadow fading model for vehicle-to-vehicle network simulations", *International Journal of Antennas and Propagation*, Article ID 190607, 12 pages, 2015.

[54] T. Mangel, O. Klemp, and H. Hartenstein, "5.9 GHz inter-vehicle communication at intersections: a validated non-line-of-sight path-loss and fading model", *EURASIP Journal on Wireless Communications and Networking*, vol. 2011, no. 1, pp. 1–11, 2011.

[55] T. Abbas, A. Thiel, T. Zemen, C. F. Mecklenbrauker, and F. Tufvesson, "Validation of a non-line-of-sight path-loss model for V2V communications at street intersections", in *International Conference on ITS Telecommunications (ITST)*, 2013, pp. 198–203.

[56] FP6 IST Project WINNER II, Deliverable 1.1.2 V1.2, "WINNER II Channel Models", 2007. [Online]. Available: `http://www.cept.org/files/1050/documents/winner2%20-%20final%20report.pdf`.

[57] M. Abdulla, E. Steinmetz, and H. Wymeersch, "Vehicle-to-vehicle communications with urban intersection path loss models", in *IEEE Globecom Workshops (GC Wkshps)*, 2016, pp. 1–6.

[58] K. Bilstrup, E. Uhlemann, E. Ström, and U. Bilstrup, "On the ability of the 802.11p mac method and stdma to support real-time vehicle-to-vehicle communication", *EURASIP Journal on Wireless Communications and Networking*, 2009.

[59] E. G. Ström, "On Medium Access and Physical Layer Standards for Cooperative Intelligent Transport Systems in Europe", *Proceedings of the IEEE*, vol. 99, no. 7, pp. 1183–1188, 2011.

[60] "Automotive vertical sector", 5G-PPP, White Paper, 2015.

[61] 5GCAR project deliverable D2.1, "5GCAR Scenarios, Use Cases, Requirements and KPIs", 5G-PPP, Tech. Rep., 2017.

[62] S. N. Chiu, W. S. Kendall, and J. Mecke, *Stochastic Geometry and Its Applications*, 3rd ed. John Wiley & Sons, 2013.

[63] M. Haenggi and R. K. Ganti, "Interference in Large Wireless Networks", *Foundations and Trends in Networking*, vol. 3, no. 2, pp. 127–248, 2008.

[64] F. Baccelli and B. Błaszczyszyn, *Stochastic Geometry and Wireless Networks, Volume I - Theory*. NoW Publishers, 2009, vol. 1. [Online]. Available: `https://hal.inria.fr/inria-00403039`.

[65] L. Hobert, A. Festag, I. Llatser, L. Altomare, F. Visintainer, and A. Kovacs, "Enhancements of v2x communication in support of cooperative autonomous driving", *IEEE Communications Magazine*, vol. 53, no. 12, pp. 64–70, 2015.

[66] G.-M. Hoang, "Cooperative multisensor localization for connected vehicles", PhD thesis, TELECOM ParisTech, 2018.

[67] H. Wymeersch, J. Lien, and M. Z. Win, "Cooperative localization in wireless networks", *Proceedings of the IEEE*, vol. 97, no. 2, pp. 427–450, 2009.

[68] E. Kaplan and C. Hegarty, *Understanding GPS: Principles and Applications*, Second. Artech House, 2005.

[69] M. R. Gholami, M. F. Keskin, S. Gezici, and M. Jansson, "Cooperative positioning in wireless networks", *Wiley Encyclopedia of Electrical and Electronics Engineering*, pp. 1–19, 2016.

[70] A. Conti, D. Dardari, and M. Z. Win, "Experimental results on cooperative uwb based positioning systems", in *IEEE International Conference on Ultra-Wideband*, vol. 1, 2008, pp. 191–195.

[71] F. d. P. Müller, "Survey on Ranging Sensors and Cooperative Techniques for Relative Positioning of Vehicles", *Sensors*, vol. 7, no. 2, 2017.

[72] A. Rauch, F. Klanner, R. Rasshofer, and K. Dietmayer, "Car2x-based perception in a high-level fusion architecture for cooperative perception systems", in *IEEE Intelligent Vehicles Symposium*, 2012, pp. 270–275.

[73] C. Mensing and J. J. Nielsen, "Centralized cooperative positioning and tracking with realistic communications constraints", in *2010 7th Workshop on Positioning, Navigation and Communication*, 2010, pp. 215–223.

[74] S. M. Kay, *Fundamentals of Statistical Signal Processing: Estimation Theory*. Prentice Hall, 1993.

[75] European Tranport Safety Council (ETSC), "BRIEFING | Cooperative Intelligent Transport Systems (C-ITS)", Tech. Rep., 2017.

[76] HIGHTS project deliverable D2.1, "Use cases and Application Requirements", Tech. Rep., 2016.

[77] *An Introduction to GNSS: GPS, GLONASS, BeiDou, Galileo and other Global Navigation Satellite Systems*, Second. NovAtel Inc., 2015. [Online]. Available: `https://www.novatel.com/assets/Documents/Books/Intro-to-GNSS.pdf`.

[78] J. Fischer, "The Role of GNSS in driverless cars", *GPS World*, 2018.

[79] S. Stephenson, X. Meng, T. More, A. Baxendale, and T. Edwards, "Network RTK for Intelligent Vehicles: Accurate, Reliable, Available, Continuous Positioning for Cooperative Driving", *GPS World*, 2013.

[80] M. I. Skolnik, *Radar Handbook*, Third. The McGraw-Hill Companies, 2008.

[81] M. Khader and S. Cherianr, "An Introduction to Automotive LIDAR", Texas Instruments, Tech. Rep., 2018. [Online]. Available: `http://www.ti.com/lit/wp/slyy150/slyy150.pdf`.

[82] S. Yuan, "Network Localization and Navigation: Theoretical Framework, Efficient Operation, and Security Assurance", PhD thesis, Massachusetts Institute of Technology, 2014.

[83] J. Rawlings, D. Mayne, and M. Diehl, *Model Predictive Control: Theory, Computation, and Design*, Second. Nob Hill, 2017.

[84] M. A. Nazari, T. Charalambous, J. Sjöberg, and H. Wymeersch, "Remote control of automated vehicles over unreliable channels", in *IEEE Wireless Communications and Networking Conference (WCNC)*, 2018, pp. 1–6.

[85] R. Hult, M. Zanon, S. Gros, and P. Falcone, "Primal decomposition of the optimal coordination of vehicles at traffic intersections", in *IEEE 55th Conference on Decision and Control (CDC)*, 2016, pp. 2567–2573.

[86] H. K. Khalil, *Nonlinear Systems*, 3rd ed. Prentice-Hall, 2002.

[87] D. Mayne, M. Seron, and S. Raković, "Robust model predictive control of constrained linear systems with bounded disturbances", *Automatica*, vol. 41, no. 2, pp. 219–224, 2005.

[88] M. Jalalmaab, B. Fidan, S. Jeon, and P. Falcone, "Guaranteeing persistent feasibility of model predictive motion planning for autonomous vehicles", in *IEEE Intelligent Vehicles Symposium (IV)*, 2017, pp. 843–848.

[89] M. P. Vitus, Z. Zhou, and C. J. Tomlin, "Stochastic control with uncertain parameters via chance constrained control", *IEEE Transactions on Automatic Control*, vol. 61, no. 10, pp. 2892–2905, 2016.